Iron mobility in shallow hydrothermal systems: insights from hematite-quartz veins and breccias from Arkaroola

Thesis submitted in accordance with the requirements of the University of Adelaide for an Honours Degree in Geology

Finnegan Birch

November 2021

THE UNIVERSITY of ADELAIDE

TITLE

Iron mobility in shallow hydrothermal systems: insights from hematite-quartz veins and breccias from Arkaroola

RUNNING TITLE

Fe mobility in hydrothermal systems at Arkaroola

ABSTRACT

A series of hydrothermal hematite and quartz veins are found within the Adelaidean cover sequence at Petalinka Waterfall and Mt Oliphant as well as within the Mt Painter Inlier in the Radium Ridge Breccia and Mt Gee Sinter. Past studies have described a genetic relationship between the Radium Ridge Breccia and Mt Gee Sinter formations. Mineral geochemistry and U-Pb monazite and hematite dating have supported this claim as well as expanded the hydrothermal history of the local area. Monazite formation at ca 360 Ma across the two locations suggests early generations of hematite at Mt Gee predate this age, with a resetting of hematite occurring around ca 300 Ma. The Mt Gee Sinter has been seen to crosscut Cretaceous tillite, giving a maximum age of this generation of hydrothermal activity of ca 220 Ma. Hematite mineral geochemistry also genetically links the hematite and quartz veins found at Petalinka Waterfall and Mt Oliphant. These veins also see multiple generations of vein formation, initiating with the Delamarian Orogeny, evident from monazite dating from Petalinka Waterfall at ca 493 Ma coupled with textural evidence from Mt Oliphant. Second generation veining has been dated using U-Pb dating of hematite, giving an age of ca 350 Ma. This suggests the geothermal conditions at ca 360-350 Ma were regional with Petalinka Waterfall hematite dates correlating with Mt Painter Inlier monazite dates. Oxygen isotope analysis of quartz and hematite suggest metamorphic sourced hydrothermal fluid at temperatures of 450^{o}C at the Mt Painter Inlier and Petalinka Waterfall and 600^{o}C at Mt Oliphant. This hydrothermal fluid was likely very saline, similar to the hydrothermal veins discussed by Bakker and Elburg (2006).

KEYWORDS

Arkaroola, Mt Painter Province, Adelaidean Cover Sequence, Iron Mobility, Hydrothermal, Vein, Breccia, U-Pb Dating, Geochemistry, Oxygen Isotope

TABLE OF CONTENTS

LIST OF FIGURES AND TABLES

Figure 15. Stratigraphic column of known relevant ages of magmatic and hydrothermal events with dates from this paper highlighted in red. 1. Delamarian Constraints by Foden (2006). 2. Alice Springs Orogeny timing by McLaren (2002). 3. Timing of RRB by McLaren (2006). 4. Pegmatites in Region by Elburg (2013). 5. Diopside and titanite veins from Bakker & Elburg (2006). 6. Cretaceous Tillite by Hore (2020)..... 42

INTRODUCTION

Arkaroola, located in the northern Flinders Ranges, is a geologically diverse terrane with events spanning over 1.5 billion years. In the north of the region are exposures of Mesoproterozoic basement rocks with high levels of uranium, creating a high geothermal gradient for the region. Exposures of Neoproterozoic metasediments dominate the region immediately to the south in and around Arkaroola village (Figure 1). This region has been heavily deformed, most notably by the Delamarian orogeny ca 515-490 Ma (Foden, et al. 2006). Associated with this deformation event is a series of pegmatites, such as the Pinnacles and Sitting Bull, as well as other smaller pegmatite outcrops dated to around 500 Ma (Elburg, et al. 2003). Finally, a series of magmatic and hydrothermal events continued throughout the region until approximately 220 Ma (Hore, et al. 2020). This activation of hydrothermal fluids is associated with radiogenic intrusions such as the British Empire Granite from ~440 Ma from the Mt Painter Inlier region (McLaren, et al. 2002, 2006).

This study focuses on a series of spectacular, decimetre- to metre-scale hematite and quartz-bearing hydrothermal veins and breccias found at Mt Gee, Radium Ridge, Petalinka Waterfall and Mt Oliphant (see Figure 1). The Mt Gee Sinter and Radium Ridge No. 2 Workings have been the focus of previous studies (Elburg, 2013), however, the hematite and quartz veins from Petalinka Waterfall and Mt Oliphant have little literature focussing on them. This study examines the petrology, geochronology, and geochemistry of each series of veins/breccias in order to establish both a genetic and temporal relationship of the veins to one another and known events occurring in the region, as well as understanding the hydrothermal conditions required to mobilise

metals such as Fe^{3+}. SEM analysis has been used to identify mineral assemblages of each sample, along with monazite, hematite, and bulk rock geochemistry of the veins and surrounding and distal host rock. Due to the high uranium content of the basement and intrusive rocks in the region, uranium-lead dating of hematite, supported by monazite uranium-lead dating was used to establish the timing of hydrothermal activity. Stable oxygen isotope analysis of the hematite and quartz from the veins has been used to identify fluid temperatures, as well as the $\delta^{18}O$ of the original fluid to give a broader understanding of fluid conditions and source (Zheng, et al. 1991). The chemical conditions of the hydrothermal fluid are also examined with substantial mobilisation of Fe^{3+}, K, U and REE, most pronounced at Radium Ridge and Mt Gee. This analysis aims to give an understanding of the veins with a consideration of local geological events (see figure 5) and their relationship to hydrothermal fluid movement within the region. This will also lead to understanding the hydrothermal conditions required to mobilise Fe^{3+} and REE to the extent found at Arkaroola, as these elements are commonly considered to be fluid immobile.

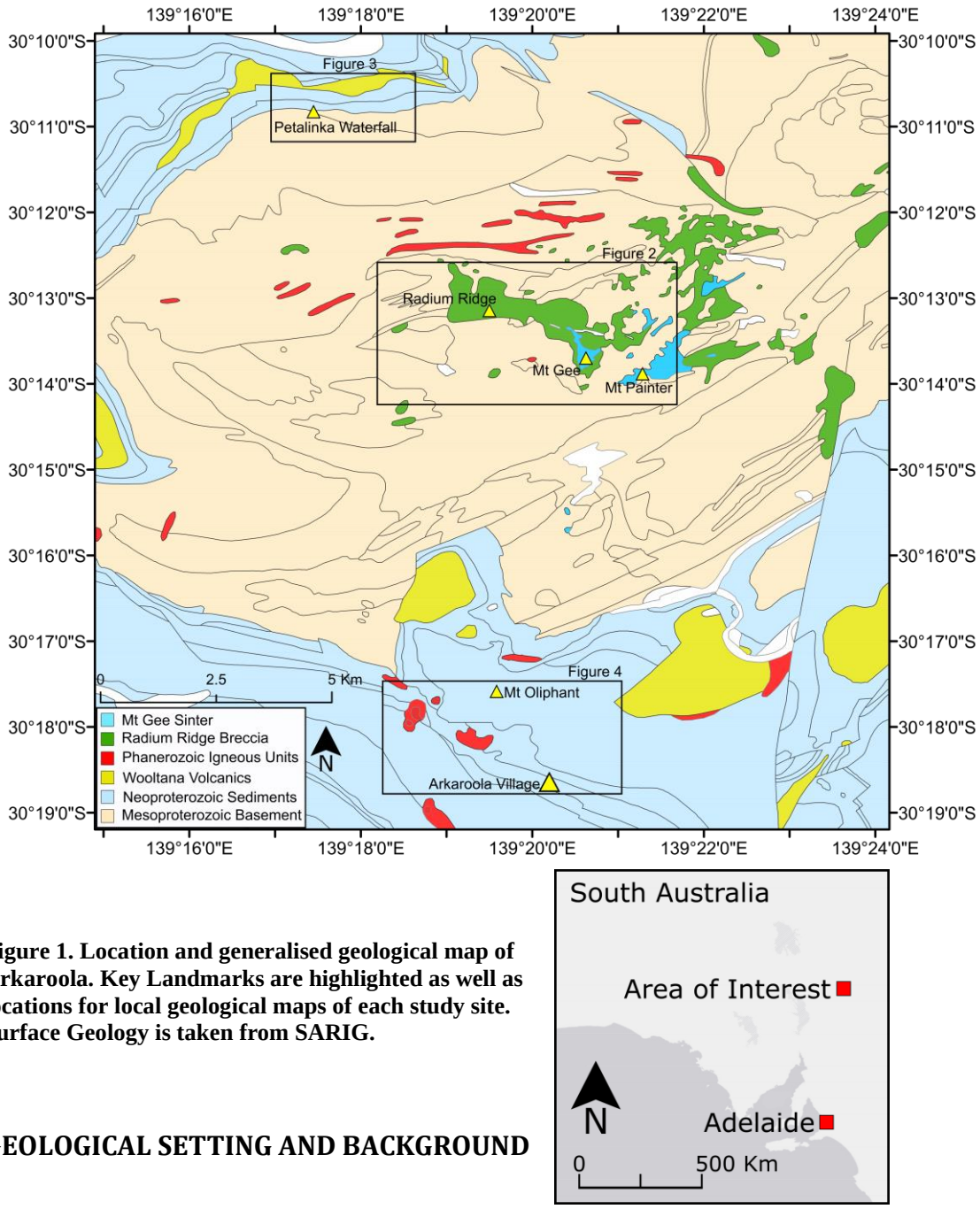

Figure 1. Location and generalised geological map of Arkaroola. Key Landmarks are highlighted as well as locations for local geological maps of each study site. Surface Geology is taken from SARIG.

GEOLOGICAL SETTING AND BACKGROUND

Local Geology

The Adelaide Fold Belt is an extensive series of mountain ranges within South Australia, encompassing the southern Adelaide Fold Belt, Nackara Arc, Central Flinders Ranges and The Northern Flinders Ranges (Lloyd, et al. 2020). Arkaroola lies within the Northern Flinders Ranges and consists of Mesoproterozoic basement, unconformably overlain by Neoproterozoic sediments deposited within a shallow,

epicontinental, rifted basin (Powel, et at. 1994). Continental breakup of Australia from Rodina at approximately 700 Ma led to passive margin conditions until the Cambrian, where continued rifting evolved into convergence and the development of the Delamarian Orogeny (Powel, et al. 1994). The sedimentary rocks in this region were metamorphosed to greenschist to amphibolite facies due to high geothermal gradients at contacts with Mesoproterozoic basement (Sandiford, et al. 1998). Continued local exhumation and deformation can be attributed to the Alice Springs Orogeny with evidence from the British Empire Granite dated at ca. 440 Ma (McLaren, et al. 2002). Evidence for hydrothermal events in the region extends across the Neoproterozoic up until as late as the mid-Cretaceous, with frequency and magnitude of hydrothermal events increasing after the Delamarian (Robinson, 1998; Hore, et al. 2020).

Mt Painter Inlier

The Mt Gee sinter and Radium Ridge No. 2 Workings lie within the region dominated by radiogenic, Mesoproterozoic basement (Figure 2), notably, the Mt Neill Granite. Stillwell and Edwards (1945) suggest a genetic relationship between Mt Gee and Radium Ridge breccia systems as well as broader systems in the area. This region is known as the Mt Painter Inlier and is characterised by pegmatite and aplite dykes crosscut by hydrothermal breccias beginning from at least 440 Ma (Bakker, Elburg, 2006). These dykes are associated with the British Empire Granite which underwent three stages of cooling at 440 Ma, 400 Ma and 330 Ma (McLaren, et al. 2002). These cooling periods are attributed to exhumation caused by the Alice Springs Orogeny (Ballèvre, et al. 2000), which also contributed to the circulation of silica, iron, potassium, uranium and REE in fluids forming the Mt Gee sinter and Radium Ridge breccia (McLaren, et al. 2006).

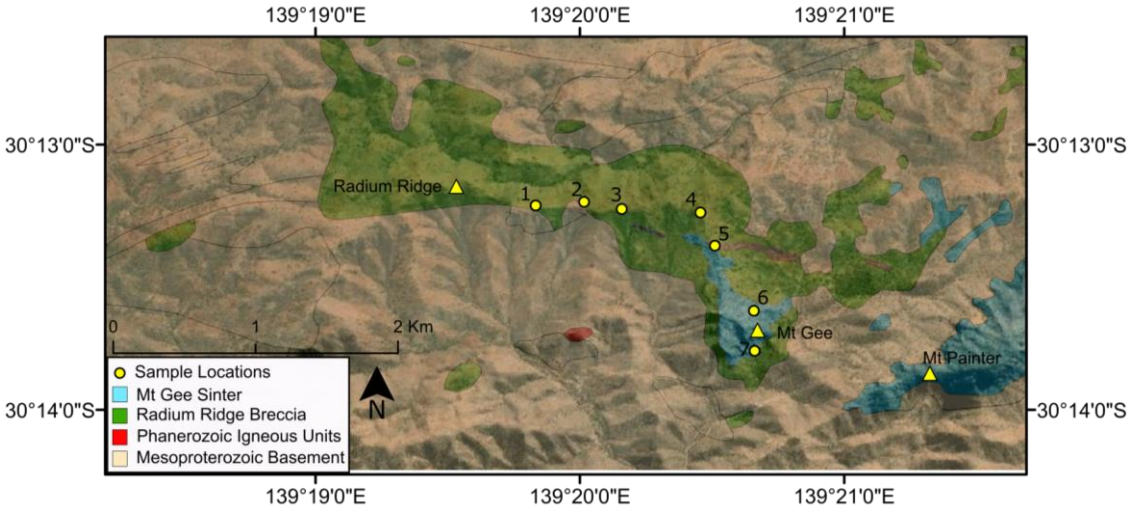

Figure 2. Local geological map of Radium Ridge and Mt Gee field site with sample locations highlighted. Note: sample location numbers correspond to Table 1 in results.

Mt Gee

The Mt Gee sinter can be characterised by a large-scale breccia spanning hundreds of metres atop Mt Gee (see Figure 2). The sinter contains two distinct mineral assemblages formed by distinct fluid alteration events (Hore, et al. 2020). The first mineral assemblage consists predominantly of hematite and quartz, with minor monazite dated at ca. 360 Ma (Hore, et al. 2020). The second generation, known as the Nail-hole quartz, due to laumontite crystal formation and dissolution, contains little hematite and monazite, and crosscuts sections of the Sprigg Tillite, from the early Cretaceous suggesting a maximum hydrothermal activity age of ca. 220 Ma (Hore, et al. 2015, 2020).

Radium Ridge

The Radium Ridge breccia is an amalgamation of granite, breccia and tillite. The breccia contains numerous sites of uranium ore prospects, such as the No. 2 Workings (see Figure 2, site 1). The No. 2 Workings deposit is situated beneath a portion of the

Nail-hole quartz from the Mt Gee sinter and is part of the Radium Ridge breccia, and therefore is genetically related to the Mt Gee sinter (Hore, et al. 2020). According to Elburg (2012), the Radium Ridge breccia includes multiple phases, pre and syn to the Mt Gee sinter, that began at 440 Ma. The No. 2 workings is associated with Fe, U and REE mineralisation and has been dated (U-Pb on monazite) to ca. 355 Ma (Elburg, 2013).

Petalinka Waterfall

The samples at Petalinka Waterfall and Mt Oliphant are situated within the Neoproterozoic metasedimentary rocks and have scarce literature focussing on them. These Neoproterozoic sedimentary rocks are part of the Adelaidean cover sequence, specifically, the Arkaroola subgroup and the lower Burra Group within the Emeroo subgroup (Job, 2011). The lithologies of these formations are predominantly pelitic in origin with intergrown sandstones, tillites, diamictites, evaporites, and carbonates (Drexel, et al. 1993). Petalinka Waterfall and the associated hydrothermal veins are located within the Freeling Heights Quartzite, Paralana Quartzite, and the Shanahan Conglomerate. These outcrops are found on the unconformable contact between the Mesoproterozoic Radium Creek group (Freeling Heights) and Adelaidean metasediments (Paralana and Shanahan).

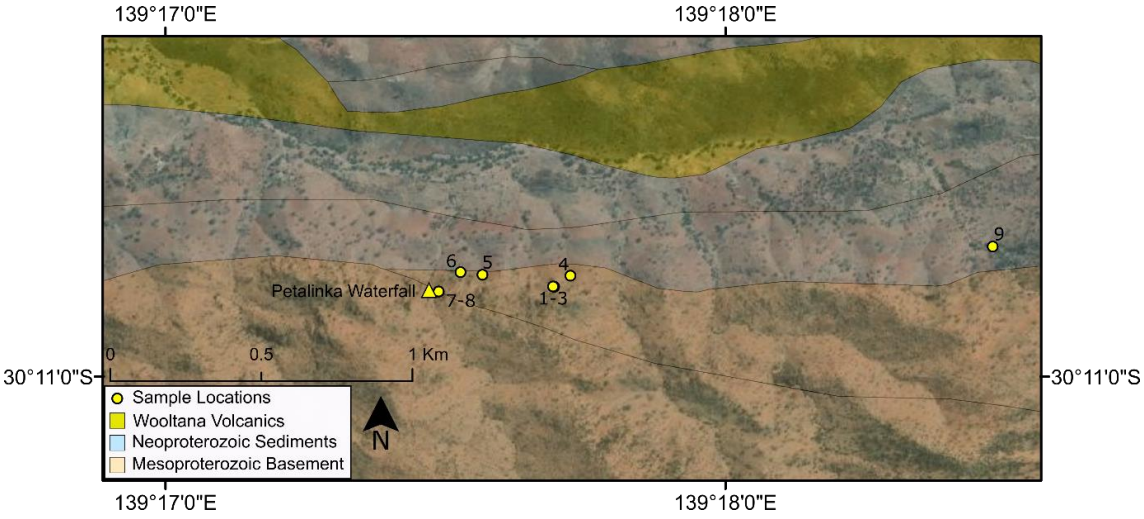

Figure 3. Local geological map of Petalinka Waterfall field site with sample locations highlighted. Note: sample location numbers correspond to Table 1 in results.

Robinson (1998) states that a set of veins found within the Freeling Heights quartzite are predominantly ilmenite and quartz-rich, rather than hematite and quartz-rich. These veins only exist within the Mesoproterozoic basement. Which indicates that this series of veins are older than the formation of the Adelaidean. The mobilisation of both titanium and iron across the different generations of veins, pre and post Cambrian, suggest similar fluid conditions in order to mobilise these normally immobile elements.

Mt Oliphant

Mt Oliphant is comprised entirely of the Woodnamocka Phyllite formation. The Woodnamocka Phyllite is a thick section of the Burra group of pelitic, evaporite origin, with characteristic millimetre, to centre metre scale foliation across the formation (Job, 2011). These sedimentary rocks are believed to experience peak deformation during the Delamarian Orogeny; however, Morphett (2013) suggests a more complex history by a series of monazite growth events within Woodnamocka Phyllite at 705.2 ±7.4 Ma and at 644.2±8 Ma, which coincides with cordierite growth within the formation (Morphett, et

al. 2013). The Phyllite varies locally, with areas of micaceous arenite, feldspar-rich arenite, associated with higher topographies, laminated, silty phyllite and coarse-grained arenite (Job, 2011). This formation is particularly magnesium-rich, predominantly containing biotite, muscovite, and sections of andalusite/cordierite (Job, 2011). These metamorphic minerals are a result of evaporite metamorphism, which has contributed to highly saline fluid mobilisation following metamorphism. Metamorphosed evaporite protoliths tend to contain minerals assemblages containing higher abundances of sodium, potassium, and magnesium (Warren, 2015). Associated with the metamorphism of these rocks, are highly saline hydrothermal fluids (Warren, 2015).

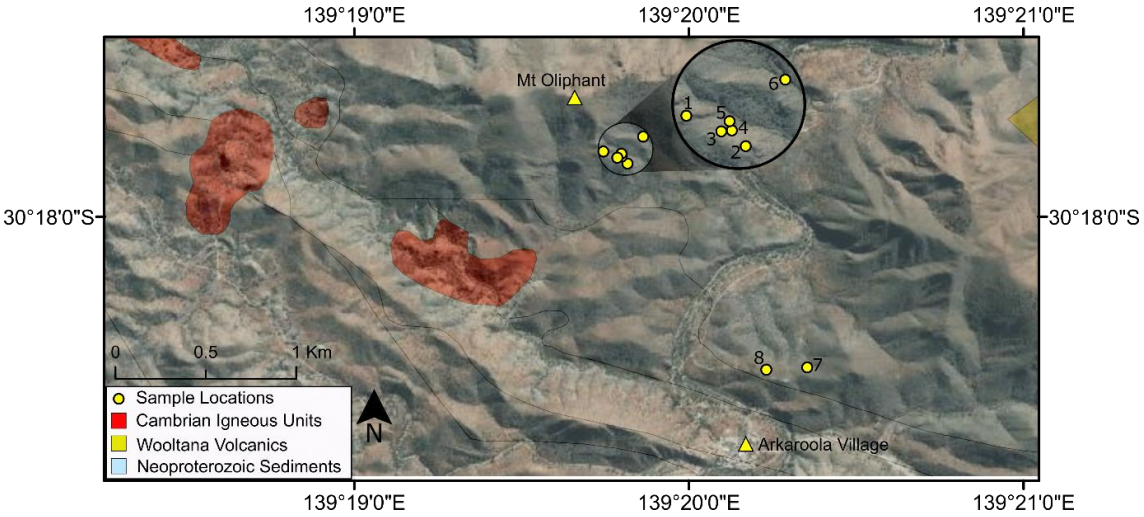

Figure 4. Local geological map of Mt Oliphant field site with sample locations highlighted. Note: sample location numbers correspond to Table 1 in results.

Fluid Conditions from previous studies

As suggested by Stillwell and Edwards (1945), genetic relationships between Radium Ridge and Mt Gee can be established, suggesting a widespread hydrothermal system. Bakker and Elburg (2006) suggest a magmatically-sourced, highly-saline (61 mass% NaCl) pegmatitic system at Mt Painter with diopside and titanite in veins formation at 443 ± 2 Ma (Bakker, Elburg. 2006) at conditions of 510 ± 20^{o}C and 130 ± 10 MPa,

followed by later stages of pure hydrothermal hematite and quartz brecciation and veining. Temperature and pressure conditions lowered following the magmatic crystallisation to 350 ± 20^{o}C and 80 ± 10 MPa (Bakker, Elburg, 2006). Salinity reduced at the transition between the magmatic and hydrothermal events to approximately 40% by mass NaCl (Bakker, Elburg, 2006). Bakker and Elburg (2006) suggest two possible mechanisms to explain the reduced salinity; "(1) preferential removal of halite crystals as the fluid system becomes saturated and; (2) addition of an external aqueous meteoric fluid" and suggest both have occurred on their studied samples (Bakker, Elburg, 2006). These highly saline fluids conditions can also be attributed to fluid from metamorphism of Neoproterozoic evaporates, such as the Woodnamocka Phyllite, and have allowed mobilisation of Fe^{3+} and other incompatible element; elements that are usually considered to be immobile under hydrothermal conditions.

Hematite bearing veins from other localities

The fluid conditions at Arkaroola are comparable to specular hematite bearing hydrothermal veins from Germany and Brazil (Cabral, et al. 2013). These veins are hosted in black shale and dolomitic BIF respectively and have propagated along existing fault lines. Similarly, to the diopside and titanite veins at Arkaroola (Bakker, Elburg, 2006), the specular hematite contains high contents of titanium (Cabral, et al. 2013). This mobilisation of hematite and titanium is also related to highly saline fluids, similar to the hydrothermal phase suggested by Bakker and Elburg (2006).

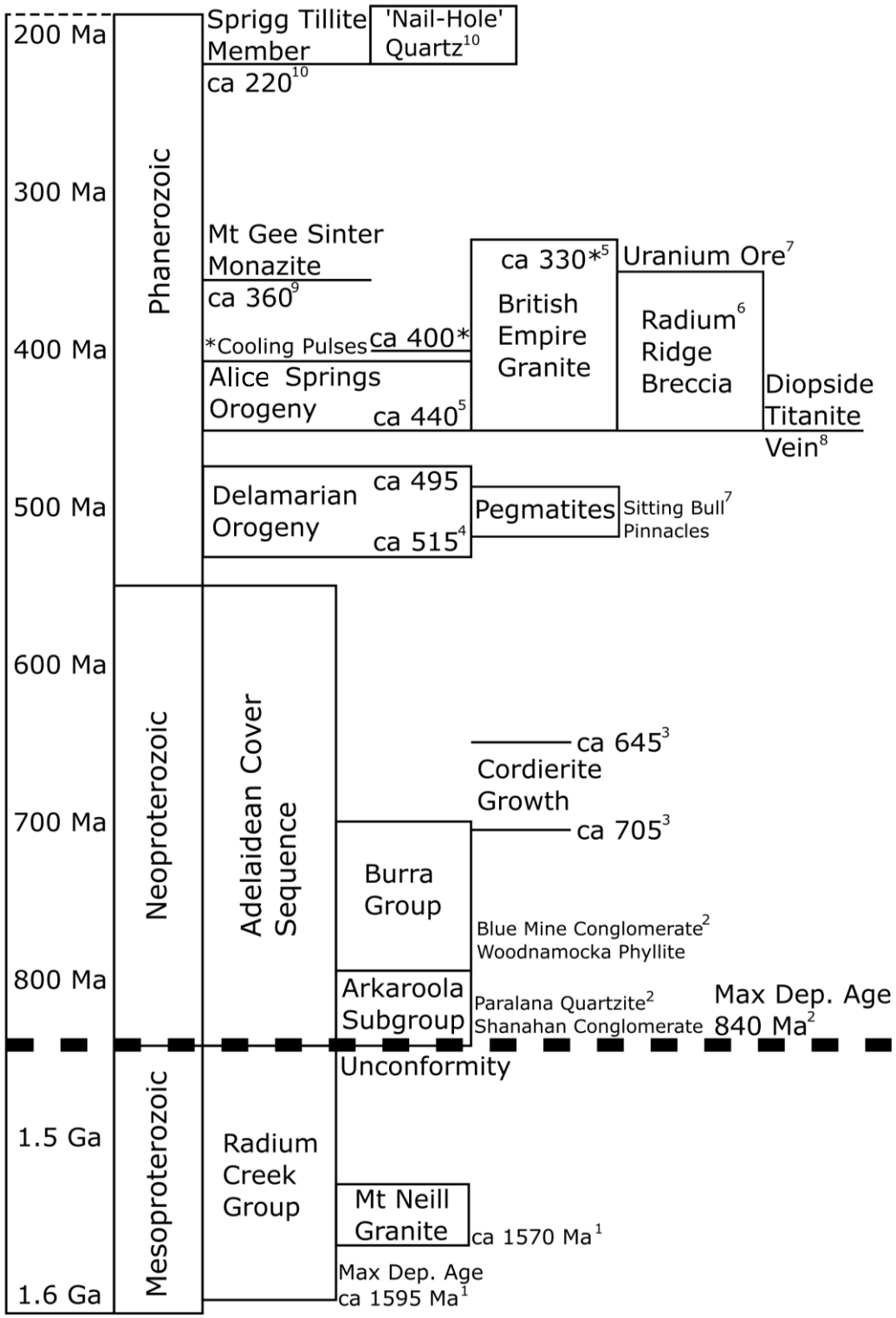

Figure 5. Stratigraphic column of relevant depositional ages, magmatic and hydrothermal events. 1. Basement timing by Armit (2014). 2. Adelaidean deposition timing. Lloyd (2020). 3. Cordierite formation by Morphett (2013). 4. Delamarian Constraints by Foden (2006). 5. Alice Springs Orogeny timing by McLaren (2002). 6. Timing of RRB by McLaren (2006). 7. Timing of RRB Ore and Pegmatites in Region by Elburg (2013). 8. Diopside and titanite veins from Bakker & Elburg (2006). 9. Monazite Ages by Hore (2020) 10. Cretaceous Tillite by Hore (2020)

METHODS

Field Work

Sample description and collection were undertaken at each field site (Figures 2-4). Sample collection included quartz hematite veins as well as host rock immediate and distal veining. GPS location and general location and rock description accompanied each sample site. Samples comprised of centi-decimetre scale boulders comprising of entirely vein rock or with sections of host rock included. Samples thought to be of different generation were categorised and labelled separately. A transect between vein and host rock from Mt Oliphant was taken to explore the extent of vein alteration.

SEM petrography

Epoxy mounted polished rock samples were analysed using a FEI QUANTA 450 scanning electron microscope equipped with energy-dispersive X-ray spectrometry (EDS) and backscattered electron (BSE) detectors. Different mineral phases were scanned to identify the elements within the phase using the EDS spectrum of each mineral analysis.

LA-ICP MS

Trace element and U-Pb geochronology analysis of hematite and monazite was conducted at Adelaide Microscopy by LA-ICP-MS using a 193 nm RESOlution-LR excimer laser microprobe (Applied Spectra) coupled to an Agilent 7900x Quadrupole ICP-MS. Acquisition protocols followed the same methodology as outlined in Courtney-Davies, et al. (2019) for natural hematite. Isotopes measured were ^{57}Fe, ^{204}Pb, ^{206}Pb, ^{207}Pb, ^{208}Pb, ^{232}Th, and ^{238}U as well as trace elements. The standards used for

hematite analysis were GSD for trace elements, HFO synthetic hematite and 91500 zircon for geochronology. The same method was followed for natural monazite samples as well, with natural standards of 222 (450 +/- 0.64 Ma), Ambat (518.5 +/- 0.71 Ma) and MAdel (518.72 +/- 0.56 Ma) for geochronology, and synthetic glass standard NIST 610 for trace elements.

Bulk Rock Geochemistry

Samples from the Mt Oliphant vein transect (Samples A170504A-D, A150505A-B) were submitted to Bureau Veritas Minerals laboratories, Vancouver, Canada, where they were milled and then analysed for major and trace elements using a combination of inductively-coupled plasma mass spectroscopy (ICP-MS) and inductively-coupled plasma optical emission spectroscopy (ICP-OES). More detail on these methods are described by Slezak and Spandler (2020).

Oxygen Isotope

Oxygen isotope analysis of 11 quartz and 11 hematite samples across Radium Ridge, Mt Gee, Petalinka Waterfall and Mt Oliphant were carried out at the Department of Geological Sciences, University of Cape Town, South Africa, using the laser fluorination methods described in Harris and Vogeli (2010). The purified O_2, formed from each sample reaction with 10 kPa BrF_5, was collected onto a 5 Å molecular sieve contained in a stoppered glass storage bottle. Isotope ratios were measured using a Finnegan Mat Delta XP mass spectrometer in dual-inlet mode. All data are reported in the standard δ-notation relative to Standard Mean Ocean Water (SMOW), where δ (‰) = ((Rsample/Rstandard) − 1) × 1000, with R being the measured ratio (e.g., 18O/16O).

RESULTS

Table 1. Summary of samples from field work. Note: sample Map # refers to marker numbers on figures 2-4.

		Figure 2	**Mt Painter Inlier Region**	
Map #	**Coordinates**	**Sample ID**	**Formation**	**Analysis Techniques**
1	30°13'14.2"S 139°19'50.5"E	A160501A-B	Radium Ridge Breccia	In situ rock ID, petrography, hematite + monazite dating + mineral chemistry, oxygen isotope analysis
2	30°13'14.6"S 139°20'09.5"E	A160502	Radium Ridge Breccia/Mt Neill Granite	In situ rock ID
3	30°13'14.1"S 139°20'21.3"E	A160503	Radium Ridge Breccia/Mt Neill Granite	In situ rock ID
4	30°13'15.2"S 139°20'24.7"E	A160504	Radium Ridge Breccia/Mt Neill Granite	In situ rock ID
5	30°13'15.4"S 139°20'27.48"E	A160505	Mt Neill Granite	In situ rock ID
6	30°13'22.8"S 139°20'29.8"E	A160506 A-F	Mt Gee Sinter	In situ rock ID, petrography, hematite + monazite dating + mineral chemistry, oxygen isotope analysis
7	30°13'44.2"S 139°20'44.1"E	Mt Gee A-B	Mt Gee Sinter	In situ rock ID, petrography, hematite + monazite dating + mineral chemistry, oxygen isotope analysis

		Figure 3	**Petalinka Waterfall**	
1	30°10'50.4"S 139°17'41.6"E	A150501A-C	Shanahan Conglomerate	In situ rock ID, petrography, hematite dating + mineral chemistry, oxygen isotope analysis
2	30°10'50.0"S 139°17'42.0"E	A150502A-B	Shanahan Conglomerate	In situ rock ID
3	30°10'50.0"S 139°17'42.0"E	A150503A-B	Shanahan Conglomerate	In situ rock ID, petrography, hematite dating + mineral chemistry, oxygen isotope analysis
4	30°10'49.2"S 139°17'43.4"E	A150504A-B	Paralana Quartzite	In situ rock ID, petrography, hematite + monazite dating + mineral chemistry, oxygen isotope analysis
5	30°10'48.8 S 139°17'31.6 E	A150505	Paralana Quartzite	In situ Rock ID
6	30°10'49.0 S 139°17'29.1 E	A150507	Paralana Quartzite	In situ Rock ID, oxygen isotope analysis
7	30°10'49.9 S 139°17'29.3 E	A150508	Paralana Quartzite	In situ Rock ID
8	30°10'49.9 S 139°17'29.3 E	A150509A-E	Paralana Quartzite	In situ Rock ID
9	30°10'46.8" S 139°18'30.4 E	A150510	Shanahan Conglomerate	In situ Rock ID

		Figure 4	Mt Oliphant Region	
1	30°17'48.4" S 139°19'44.7 E	A170501	Woodnamocka Phyllite	In situ Rock ID, oxygen isotope analysis
2	30°17'50.4"S 139°19'49.1"E	A170502	Woodnamocka Phyllite	In situ Rock ID, oxygen isotope analysis
3	30°17'49.3"S 139°19'48.0"E	A170503A-D	Woodnamocka Phyllite	In situ Rock ID, oxygen isotope analysis, thin section
3	30°17'49.3"S 139°19'48.0"E	MasHem, QHV	Woodnamocka Phyllite	In situ rock ID, petrography, hematite + monazite dating + mineral chemistry, oxygen isotope analysis
4	30°17'49.4"S 139°19'49.4"E	A170504A-C	Woodnamocka Phyllite	In situ rock ID, petrography, bulk rock chemistry, thin section
5	30°17'49.4"S 139°19'49.4"E	A170504D	Woodnamocka Phyllite	In situ rock ID, petrography, bulk rock chemistry
6	30°17'49.1"S 139°19'49.4"E	A150505A-B	Woodnamocka Phyllite	In situ rock ID, petrography, bulk rock chemistry
7	30°18'27"S 139°20'21.2"E	A170506	Blue Mine Conglomerate	In situ rock ID
8	30°18'27.4"S 139°20'13.9"E	A170507A-E	Blue Mine Conglomerate	In situ rock ID, petrography, oxygen isotope analysis

Rock Description and Petrography

Radium Ridge

The samples from Radium Ridge lie within the Radium Ridge Breccia. Samples A160501A-B were at the location of the No. 2 Workings. This outcrop is predominantly a ten-metre scale, massive hematized breccia of quartz and hematite. Sections of Spriggite (Pb_3 $[(UO_2)_6O_8(OH)_2](H_2O)_3$, Brugger, 2004) mineralisation are present (Figure 6a). This location was also beneath a section of Nail-hole quartz from the Mt Gee sinter. Sample A160501A-B contained approximately 60% hematite with grain size varying from tens of micron to millimetres in scale. These larger grains were very euhedral and had extremely metallic lustre. Quartz was intergrown with the finer-grained hematite and created sawtooth patterns at ten-micron scales. Overall, quartz contributed to approximately 15% of the overall rock and was commonly included within monazite and spriggite grains. Large, euhedral grains of spriggite (Figure 6a), up to millimetres in scale, dominated portions of the sample, up to approximately 15%.

These grains were bright yellow/orange and were surrounded by the euhedral hematite crystals. Monazite made up approximately 10% of the rock. These monazite grains were yellow/brown and commonly millimetre in size, but most were hundreds of microns in size (Figure 6b). The smaller grains of hematite and quartz surrounded the sections that contained monazite. Parts of the monazite grains were broken up and intergrown with the hematite and quartz. Barite grains, at micron-scale, were also present throughout the rock, to a very minor degree. Samples A160502-A160505 were sections of hematized granite, which likely are altered sections of the Mt Neill Granite or the British Empire granite.

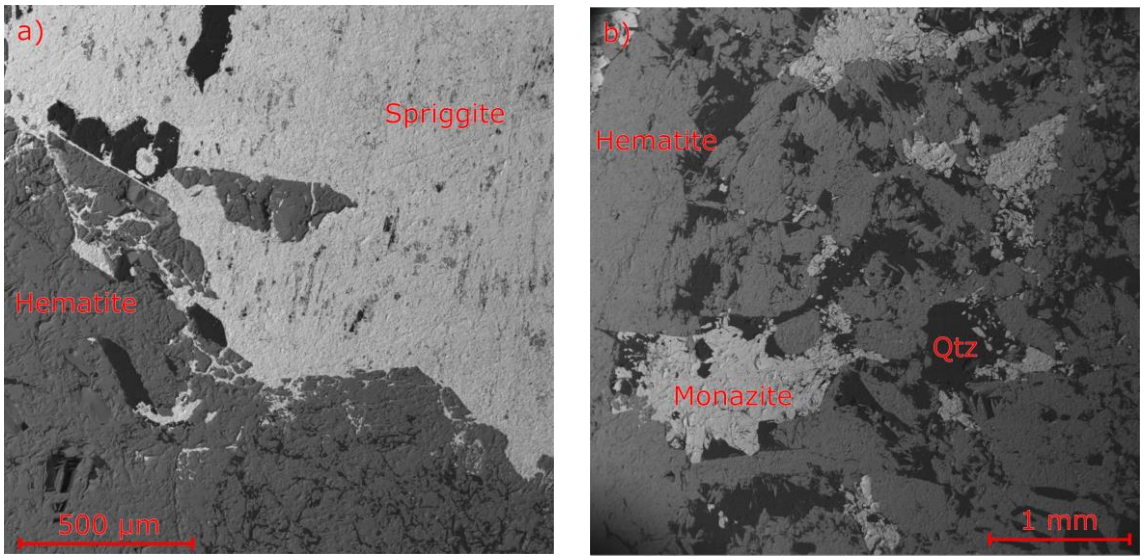

Figure 6. a) Spriggite mineralisation within No. 2 workings sample. b) SEM image of sample A160501A with labelled mineral phases

Mt Gee

Samples A160506A-F and Mt Gee A-B represent the Mt Gee sinter and the different generations that make up the breccia. This outcrop consists of multiple generations of hematite and quartz. The first generation of hematite forms massive, euhedral, centre metre-scale clasts. The second generation of hematite is coupled with quartz and is from the second hydrothermal event at Mt Gee. This generation of hematite is a brown/red

section of earthy hematite and is much less massive than the earlier generation of hematite and is intergrown with quartz. This generation of quartz also commonly separates the early generation of hematite from the earthy hematite (Figure 7a). The last hydrothermal event at Mt Gee consists of only quartz. This generation brecciates the previous generation of the sinter and is what makes up the Nail-hole quartz with dissolved laumontite and hence, is more porous than the previous quartz generations. (Figure 7b)

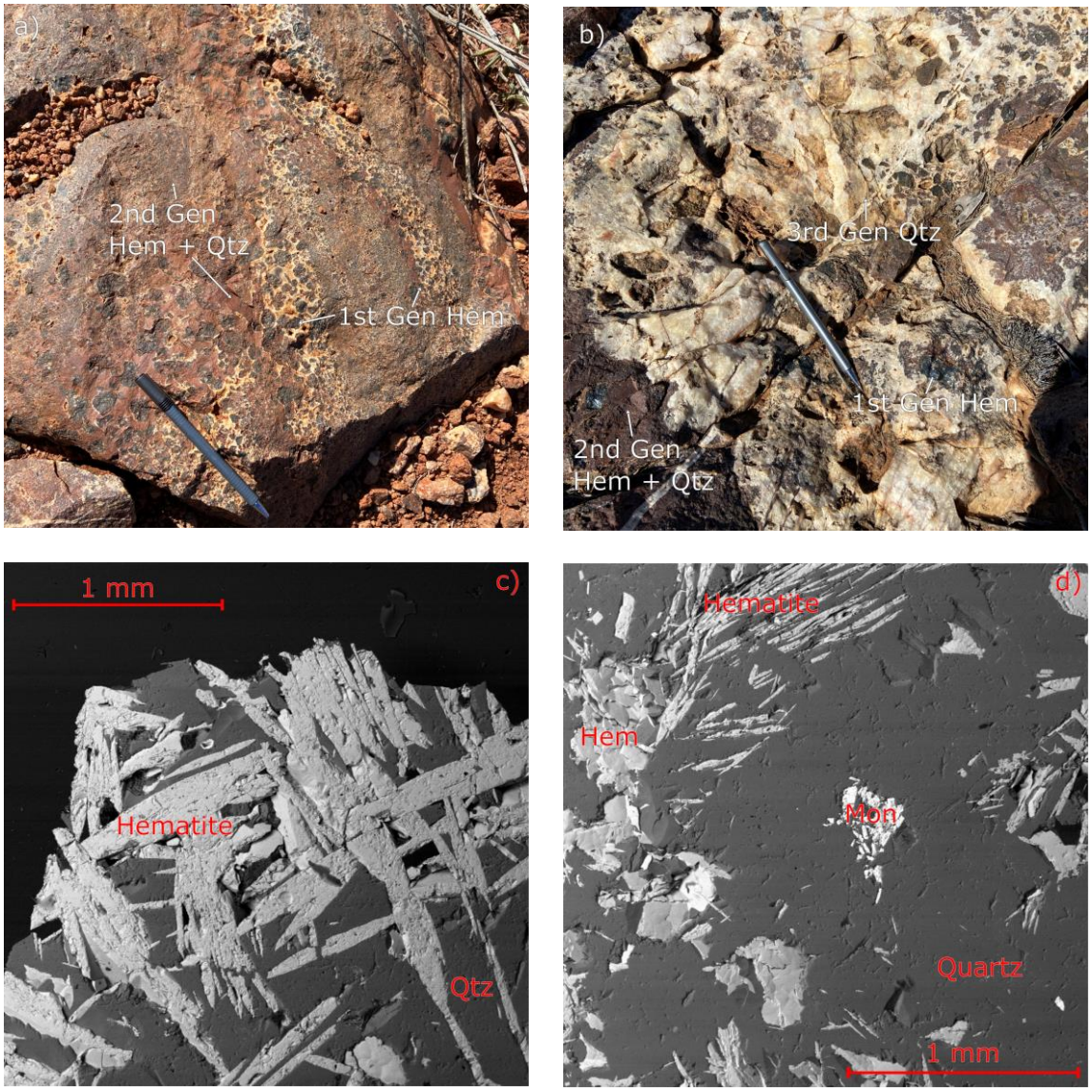

Figure 7. Mt Gee Sinter. a) Mt Gee Sinter: First generation of hematite and second generation of earthy hematite with quartz. b) Last generation of hematite poor quartz crosscutting older generations. c) SEM image of early generation hematite from sample A160506. d) SEM image of monazite within earthy hematite and quartz from sample A160506.

Sample A160506 was an amalgamation of the different phases from Mt Gee, containing the early generation of massive hematite chunks, as well as earthy hematite, associated with the first generation of quartz. This section contained no late generation, nail-hole quartz. These massive hematite chunks were predominantly intergrown, euhedral, acicular hematite and quartz. Sawtooth patterns at ten-micron scale were also very common. These sections were approximately 70:30 hematite to quartz and made up an overall 40% of the rock (Figure 7c). The remaining section of the rock was made up of the second generation of hydrothermal activity. The earthy hematite sections were a deep red, intergrown with pure white quartz veins and were predominantly quartz with micron to ten-micron scale hematite. Within the quartz veins and earthy hematite section, ten-micron scale monazites could be found (Figure 7d). The monazite was only associated with this hydrothermal generation and not the early hematite sections. Samples Mt Gee A and B were similar to A160506 but contained a larger proportion of the earthy hematite at about 80% earthy hematite/quartz vein to 20% early hematite generation. This sample also contained similar amounts of monazite to A160506.

Petalinka Waterfall

The samples from Petalinka Waterfall are found in the Shanahan Conglomerate as well as close to the boundary of the Paralana Quartzite and the Mesoproterozoic Freeling Heights Quartzite. The veins are predominantly quartz and hematite rich, with sections with distinctive sawtooth patterns between hematite and quartz (Figure 8a) and other sections of decimetre-scale quartz and hematite (Figure 8b). Samples A150501A-C are clasts of hematite and quartz that appeared to be within the matrix of the Shanahan Conglomerate, suggesting this clast is older than the Neoproterozoic deposition of this formation (Figure 8c). A150501A was a five-centimetre pebble that was approximately

75% quartz and 25% euhedral, acicular hematite. Suspended within the quartz were sub-micron scale zircons. Samples A150502 A-B and A150503 A-B are quartz hematite veins found within the Shanahan Conglomerate. Sample A150503A contained the hematite and quartz veins, as well as a section of the Shanahan Conglomerate host rock. This sample was approximately 50% pure quartz and 50% intergrown quartz, biotite, and acicular hematite. The hematite sections were about 70% hematite, 20% quartz and 10% biotite. The host rock was predominantly quartz, K-feldspar, and biotite in equal ratios. Hematite crystals at ten-micron scale were intergrown in this matrix with monazite included. Samples 150505-150509A-E are all quartz and hematite veins from the Paralana Quartzite. These samples are all similar, with centimetre to decimetre scale hematite and quartz veins, with no obvious orientation. Samples A150504A-B found within the Paralana Quartzite are noticeably different to the other veins in the area. This was due to the outcrop being distinctly hematized and with a more obvious orientation to the vein structure (Figure 8d). The more hematized sections were visually different to the vein rich sections. Sample A150504A was a heavily hematized section of a quartz and hematite vein. The vein was quartz, biotite, and hematite rich with abundant monazites at ten-micron scale. The sections of hematite were millimetre in scale and euhedral. Biotite and quartz were intergrown with one another with large amounts of monazite suspended within. Hematite made up approximately 35% of the rock, with at least 60% split between biotite and quartz and at least 5% of monazite, showing how monazite rich this vein was. Sample A150504B was a section with more quartz veining and less hematization. Evident from SEM imagery, this sample was a very biotite rich vein of quartz and hematite. The hematite in this sample was very euhedral, acicular, and hundred-micron scale and was much less abundant when compared to all other

veins, with approximately 15% of the rock being hematite. Biotite made up approximately 40% of the rock, with triangular-shaped, euhedral, hundred-micron scale grains. The remaining 45% of the vein was made up of quartz bearing trace amounts of micron-scale monazite. Samples A150510 are a section of heavily hematized Shanahan Conglomerate. This outcrop has centimetre scale quartz and feldspar clasts within a matrix of hematite (Figure 8e). Section of veining are also much more deformed in this area (Figure 8f).

Figure 8. Petalinka Waterfall. a) Sawtooth pattern from hematite and quartz veins. b) Decimetre scale veining of hematite and quartz. c) Hematite and quartz clast found within Shanahan Conglomerate. d) Hematized vein with more obvious structure. e) Hematized Shanahan Conglomerate. f) Deformed quartz vein within Shanahan Conglomerate.

Mt Oliphant

The Mt Oliphant samples are found within the Woodnamocka Phyllite. The veining shows evidence for multiple generations of hydrothermal activity. This is evident through centimetre-scale hematite and quartz veins that are foliated with the host rock striking 340^{o} to 10^{o}. A distinct second generation of decimetre-scale hematite and quartz veins crosscut the foliation and the earlier generation of veins. Surrounding the veins are chloritic altered sections of host rock that were extremely brittle underfoot. Figure 9 represents the generational vein relationship with the surrounding chloritic alteration zone and host rock.

Samples A170501 – A170503A-B, MasHem and QHV are all vein samples from the study site. Sample MasHem was a section of a massive hematite boulder from Mt Oliphant. This sample consisted of at least 75%, very coarse-grained, euhedral hematite, intergrown with biotite and quartz. The quartz and biotite were also euhedral and coarse-grained and seems to have grown in pores of the hematite. Sections of the

hematite were heavily fractured and porous, allowing quartz and biotite to infill. Sample QHV was a section of the second-generation hydrothermal vein from Mt Oliphant. The quartz and hematite in this sample were millimetre scale, very coarse and euhedral grains with very little inclusions within the crystals. The hematite was more fractured and porous than the quartz but there was no infilling textures like the MasHem sample. Samples A170503C+D are from the surrounding host rock and chloritic alterations zones.

Samples A170504A-D are a transect from within the vein, to the chlorite alteration zone from a pinched-out section of veining to the host rock, distal to any alteration. Sample A170504B was a section of the first-generation hydrothermal vein from Mt Oliphant as well as a section of altered host rock. The vein itself was similar to QHV, with very coarse, euhedral hematite and quartz as well as plagioclase, biotite, and muscovite growth within the fractures of hematite. The host rock within this sample contained predominantly foliated muscovite, biotite, K-feldspar, and quartz in a matrix. Small grains of hematite and apatite were common within the matrix of the host rock. The vein in this sample was also foliated at a millimetre scale along with the host rock.

Sample A170504C was a section of chloritic alteration approximately 5 metres below the series of veins from Mt Oliphant. The veining in this section appeared to pinch out into only chloritic alteration. This sample was made up of a matrix of biotite, muscovite, and chlorite in equal quantities of about 20% and approximately 10% quartz. This matrix was full of monazite and apatite, with some apatite crystals being millimetres in scale. The monazite was much smaller grained at micron scale. Larger grained monazites were commonly associated with the apatite and chlorite grains.

Samples A170504D and A170505A-B were host rock phyllite from the Woodnamocka Phyllite. These samples were predominantly a matrix of biotite, muscovite, and quartz and were foliated at millimetre scales. Minor amounts of fine-grained hematite were also distributed throughout the matrix as well as apatite, zircon, and monazite to a lesser extent. Most of the rock was porous, however, zones of more densely packed material, that, with a naked eye, looked like separate grains were also abundant. This is likely from clasts of more competent material from the original, unmetamorphosed host rock. Samples A170504D and A170505B also contained abundant red cordierite clasts at millimetre scale. Figure 9 shows a schematic representation of the vein system at Mt Oliphant with samples bulk rock analysis of samples A170503C-D, A170504C-D and A170505A-B.

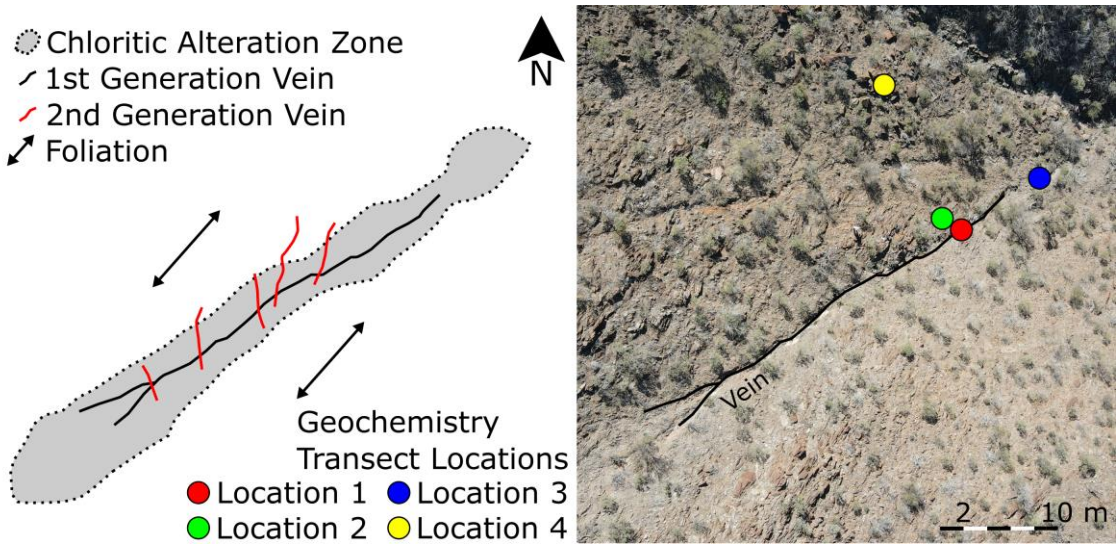

Figure 9. Schematic diagram of vein-host rock relationship and alteration extent from Mt Oliphant. Location 1: Sample A170503C, Location 2: A170503D, Location 3: A170504C, Location 4: A170504D. See Figure 11 for bulk rock trace element abundance.

At the boundary of the Woodnamocka Phyllite and Blue Mine Conglomerate (Figure 4, location 7 and 8), a section of a hematite and quartz vein (sample A170506), reminiscent to the Mt Oliphant veins outcrops, as well as a series of hematite, quartz, and talc veins (Figure 10 – Sample A170507A-E). The hematite, quartz, and talc outcrop was approximately 2 square metres in size. Approximately 80% of the vein was dominated by massive, blocky hematite and was not commonly intergrown with talc and quartz, with sections of hematite being up to metre scale thick. This hematite was fractured, which saw infilling of quartz and talc at a microscopic level. Associated with this quartz veining was minor rutile grains at micron scales. This rutile was always associated with quartz and was not very common. The hematite vein had sections of much more competent material and was not fractured as much in these regions, and therefore, quartz and talc were much less abundant in these sections.

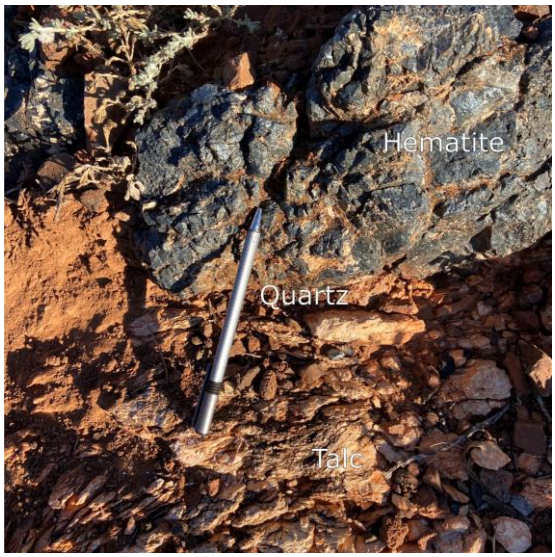

Figure 10. Blue Mine Conglomerate: Hematite, quartz, and talc vein.

Geochemistry of Vein Transect

A transect from the Mt Oliphant from chloritic altered host rock and further unaltered host rock was analysed for bulk chemistry elemental abundances (Transect from Figure 9). This was to explore the alteration extent and effect of the vein in the local area. Figure 13 shows an enrichment in SiO_2 and MgO and a depletion of Al_2O_3 in the alteration zone (0 metres). The local host rock (1 metre) is enriched in Fe_2O_3 and depleted in all other oxides. With the pinched-off region of the chloritic alteration (5 metres) comparable to the distal host rock (>10 metres).

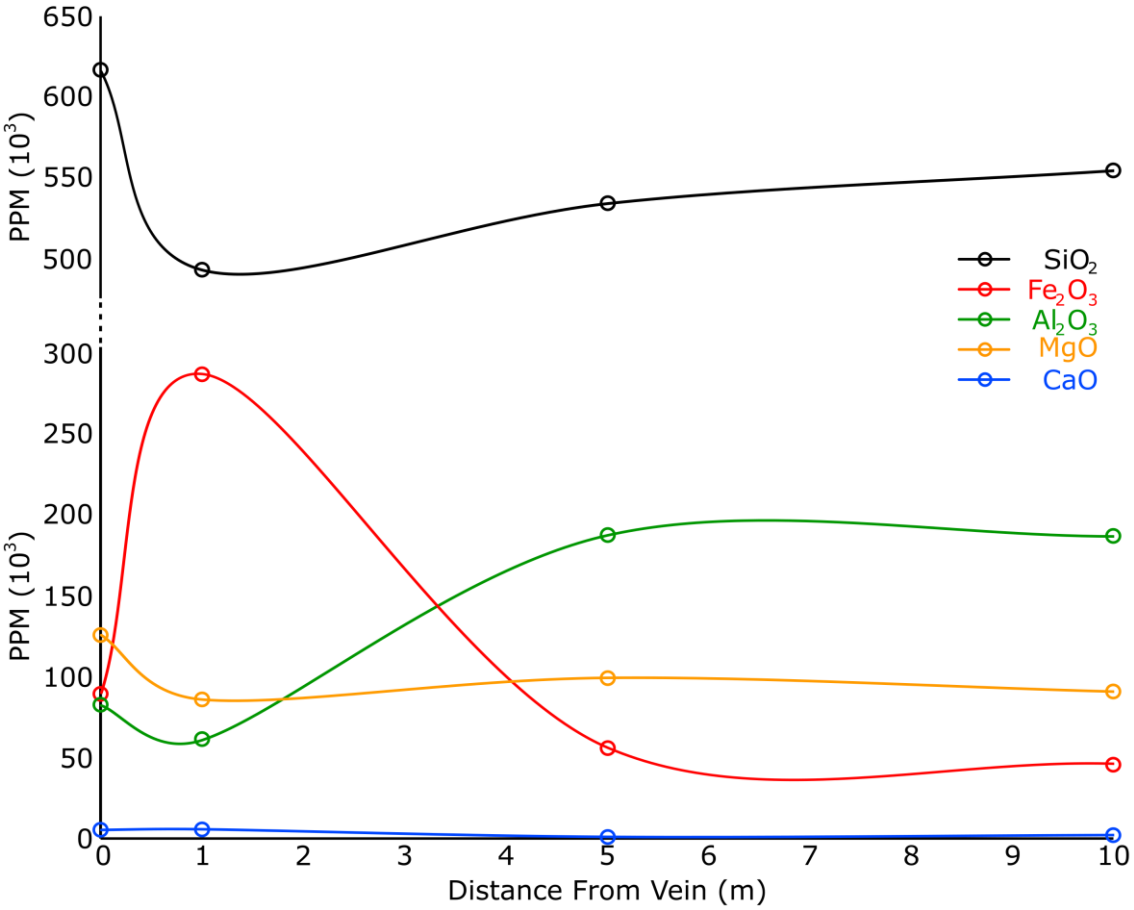

Figure 11. Scatter plot of distance from vein vs concentration (ppm) of bulk rock oxide abundancies from vein transect (Figure 9). Distance from vein coincide with labels from Figure 9; Location 1 = 0 m, Location 2 = 1 m, Location 3 = 5 m, Location 4 = >10

Geochemistry of Hematite and Monazite

In situ hematite crystal phases were analysed by LA ICP-MS to attain U-Pb geochronology dates due to the high uranium content in the region, as well as trace element abundances (Figure 12). The results of this trace element analysis show samples from similar regions having the similar abundances of specific elements. The samples from Petalinka Waterfall and Mt Oliphant also seem to closely match one another with specific trace elements within the hematite while samples from Radium Ridge and Mt Gee also match one another. This is particularly noticeable for elements such as Ti, Cr, and V being enriched at Mt Oliphant and Petalinka waterfall and with Y and other REE enriched at Mt Gee and Radium Ridge Samples.

In situ monazite grains were analysed through ICP-MS to attain U-Pb geochronology dates as well as trace element abundances normalised to average chondrite abundances. The overall REE trend of these monazites shows enrichment in LREE and depletions in HREE, as expected for monazite. Samples A160501A-B (Figure 13a-b) from the No. 2 Workings show a distinct separation in monazite populations, with one set being enriched in HREE when compared to the other population. Samples A160506 and Mt Gee A from Mt Gee (Figure 13c-d) have considerably more variation between monazite populations. Sample A150504A (Figure 13e) had considerably less variation in the monazite population.

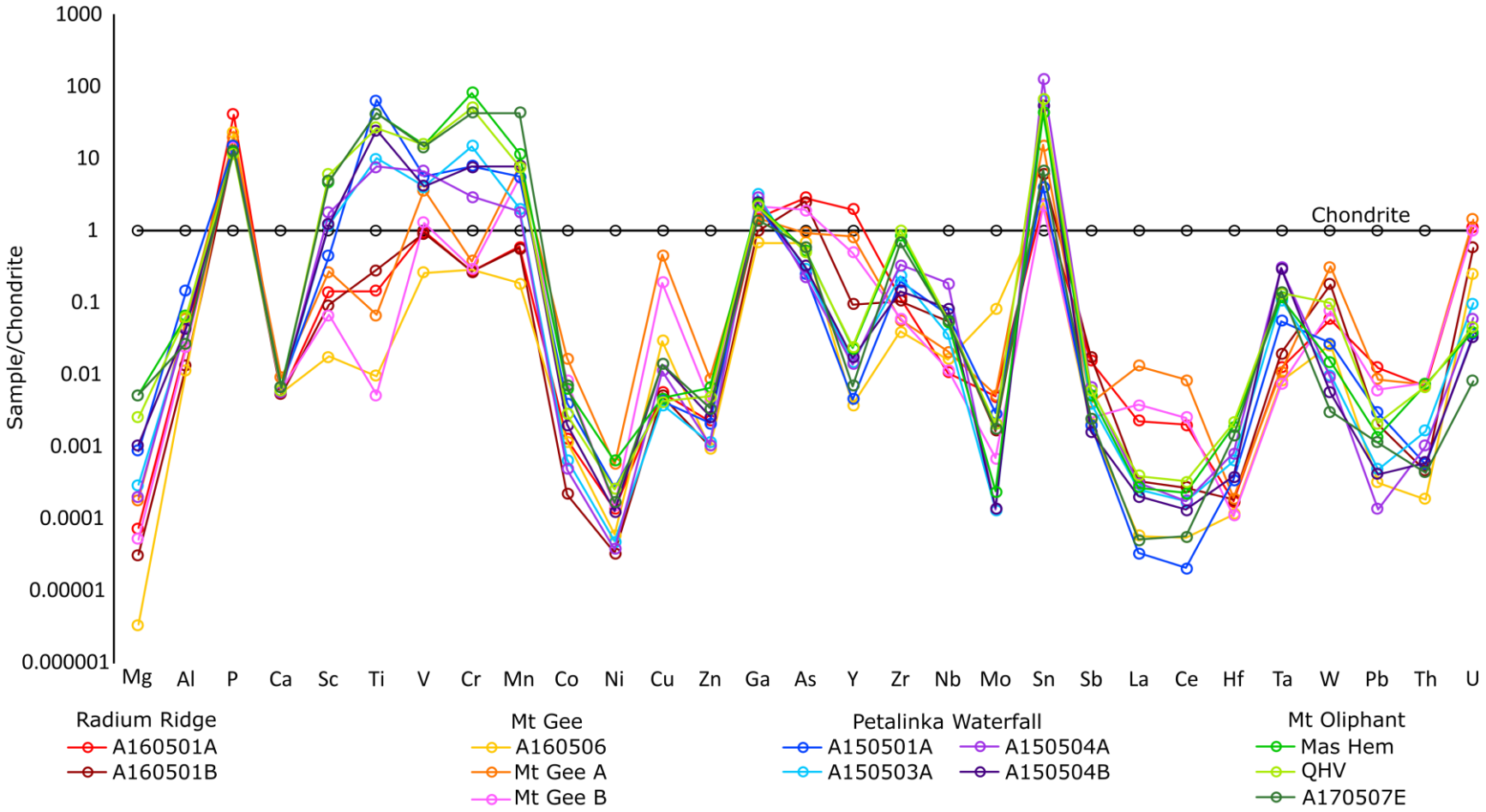

Figure 12. Trace element of hematite plot normalized to average Chondrite (McDonough, 1995). Samples A160501A-B from the No.2 Workings from Radium Ridge. Samples A160506, Mt Gee A-B from the Mt Gee sinter. Samples A150501A, A150503A, A150504A-B from Shanahan Conglomerate/Paralana Quartzite near Petalinka Waterfall. MasHem and QHV from Mt Oliphant and A170507E from the contact between the Woodnamocka Phyllite and Blue Mine Conglomerate

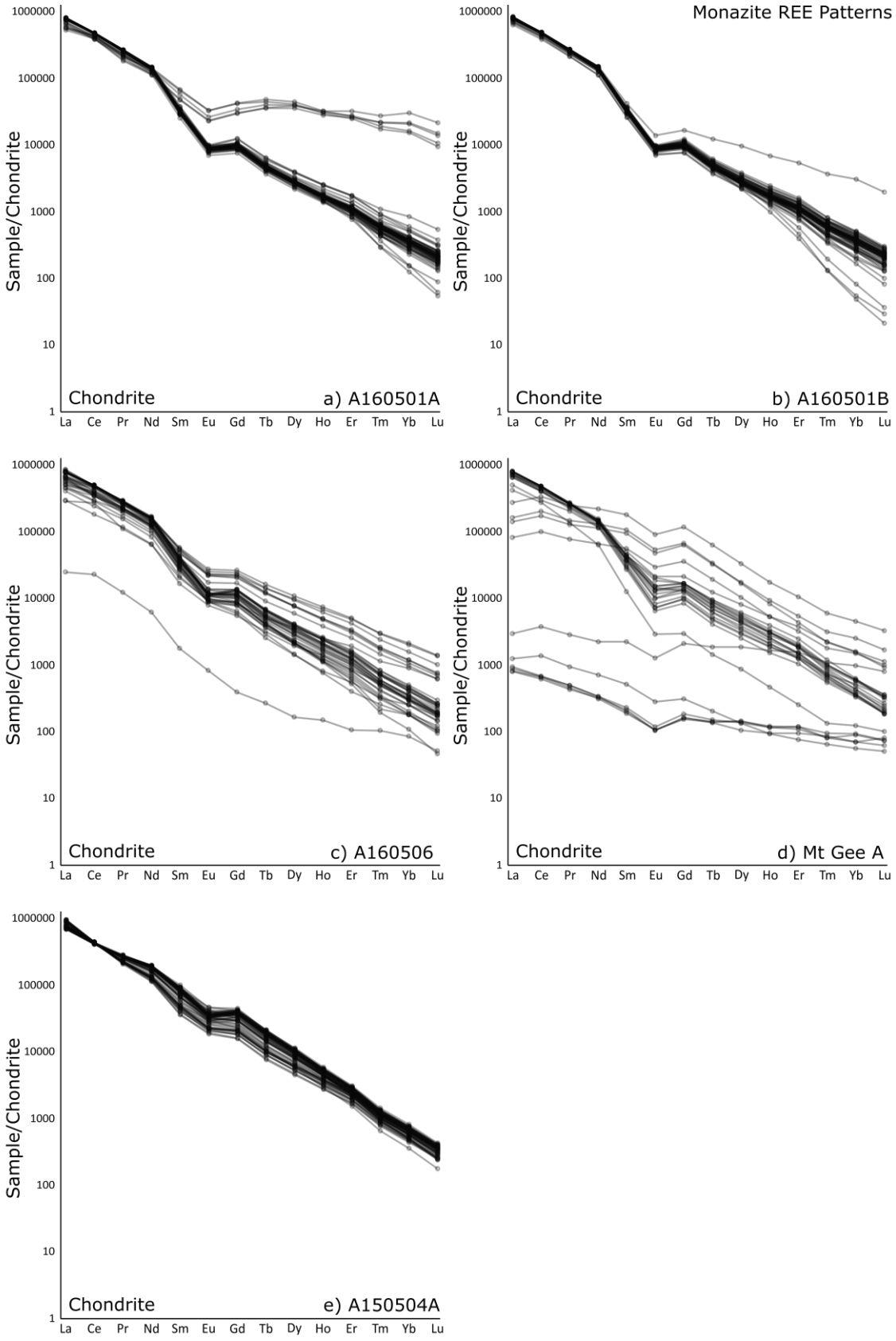

Figure 13. Monazite REE pattern for each sample normalised to average Chondrite compositions. (McDonough, 1995). a and b from No. 2 Workings from the Radium Ridge Breccia. c and d from Mt Gee. e from hematized section at Petalinka Waterfall.

Oxygen Isotope

Crystals of hematite and quartz were analysed for their $\delta^{18}O$ values. The difference between each mineral such as quartz and hematite fractionation values can be used to calculate the original temperature of fluid at the time of formation as well as the original fluid $\delta^{18}O$ value (Vho, 2019), provided the quartz and hematite were formed under equilibrium conditions.

Table 2. Results from oxygen isotope analysis with laboratory δ18O acquired date and calculated temperatures and original fluid δ18O. Temperature error of 14.4% calculated from fractionation uncertainties from Vho, 2019. *Results that are unlikely or impossible.

Sample Location	Quartz $\delta^{18}O$	Hematite $\delta^{18}O$	Calc. Temp. (^{O}C)	Error (+/-^{O}C)	Original Fluid $\delta^{18}O$
A160501A-B Radium Ridge	8.32	-2.87	420	60	4.58
A160506A-B Radium Ridge	0.23	2.00	Impossible	-	-
A160506C Mt Gee	-1.76	-5.91	1340*	190	-1.28*
A150501A-C Petalinka	11.10	0.04	430	60	7.47
A150503A-B Petalinka	11.34	2.04	530	80	9.15
A150504A Petalinka	11.70	1.84	500	70	9.07
A150507 Petalinka	11.70	0.77	430	60	8.19
A170501 Mt Oliphant	15.40	12.54	1980*	290	13.21*
A170502 Mt Oliphant	15.51	6.66	570	80	13.65
A170503A Mt Oliphant	15.74	7.29	600	90	14.16
A170507D Bluemine Boundary	16.30	8.29	640	90	15.01

Results were evaluated on the basis of reasonable temperature values and repeatable isotope values across the same sample location. Analytical errors are not taken into consideration, and therefore, temperature values are given to the nearest ten ^{o}C. Impossible temperature outcomes indicate a disequilibrium between hematite and quartz crystallisation and therefore, these results are null. The samples from Radium Ridge and Petalinka waterfall have similar fluid temperatures of around 450^{o}C while the Mt Oliphant samples are significantly higher in temperature of around 600^{o}C. Samples A160506A-B, A160506C and A170501 gave impossible values, as these temperatures calculated are above formation temperatures of hematite and quartz and therefore, these minerals would not be forming at these temperatures. All calculated original fluid δ^{18}O are positive values around, 8 at Petalinka Waterfall and around 14 for Mt Oliphant.

Geochronology

In situ hematite and monazite were dated in situ by U-Pb using LA ICP-MS. Hematite dating was used as the region is known for its enrichment in uranium. Monazite dating was used to crosscheck and confirm these results in samples that contained large enough monazite crystals. Due to the relatively new technique of U-Pb hematite dating and uncertainty within the standards used, results from this analysis are not fully reliable and are used as a rough guide and not precise ages for dating the hematite formation. Some samples had common lead inclusions, heavily skewing U-Pb dates and therefore these samples were not useful. Furthermore, some samples contained uranium content below detection limits and were not useful. Due to these considerations, data points not concordant on Terra-Wasserburg concordia plots were filtered out. Concordia plots and age histograms can be seen in Figure 14 with summary ages and associated error in table 3.

14 a) Radium Ridge: A160501A

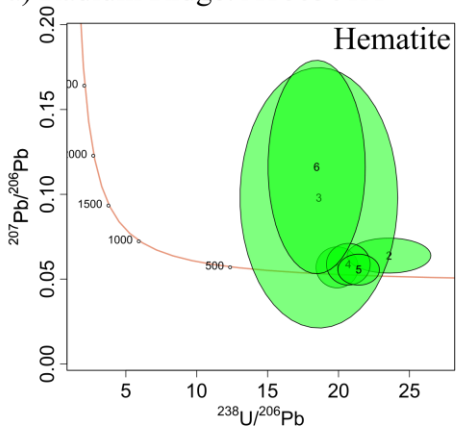

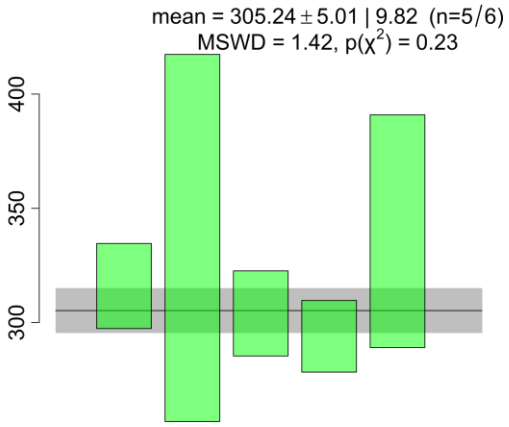

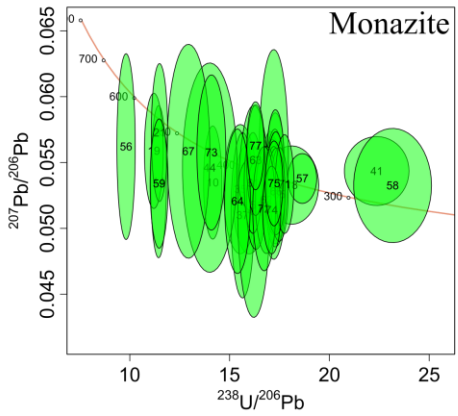

14 b) Radium Ridge: A160501B

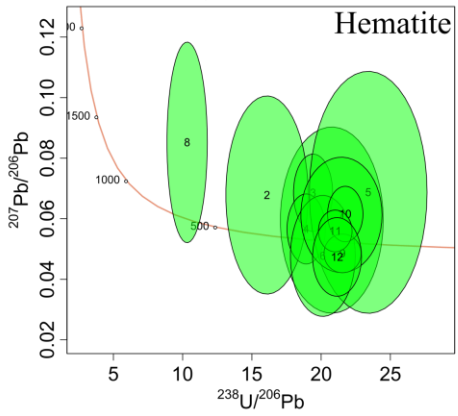

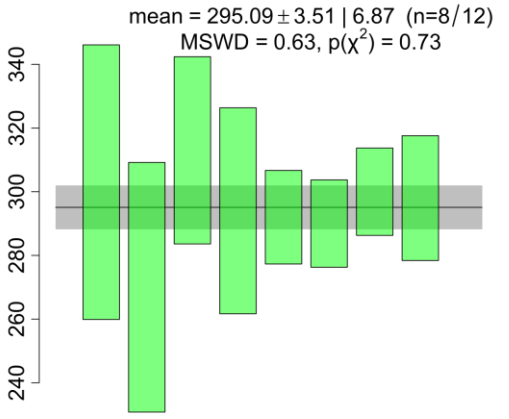

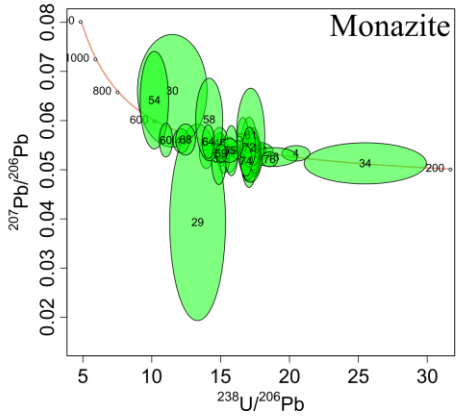

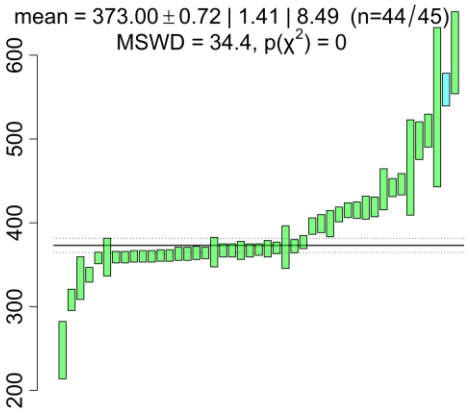

14 c) Mt Gee: A160506

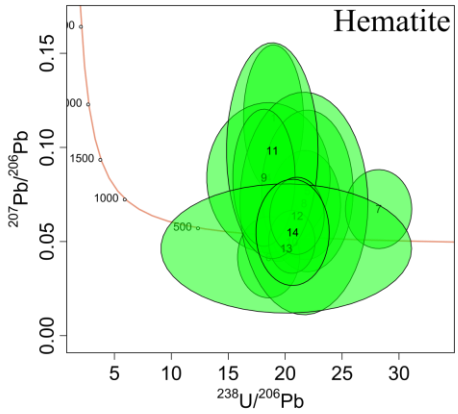

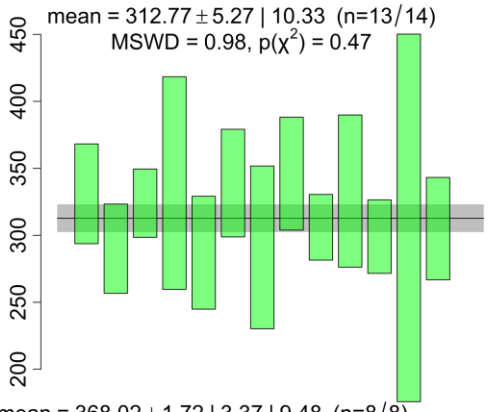

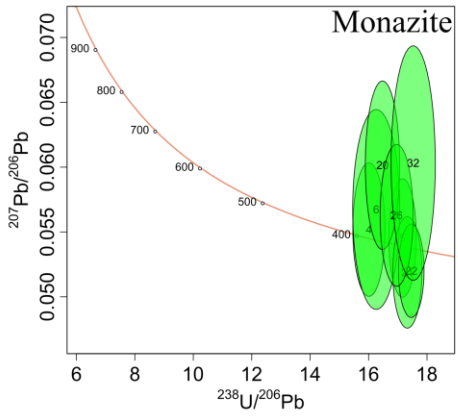

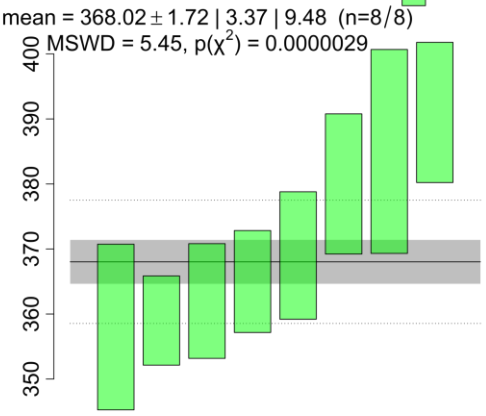

14 d) Mt Gee: Mt Gee A

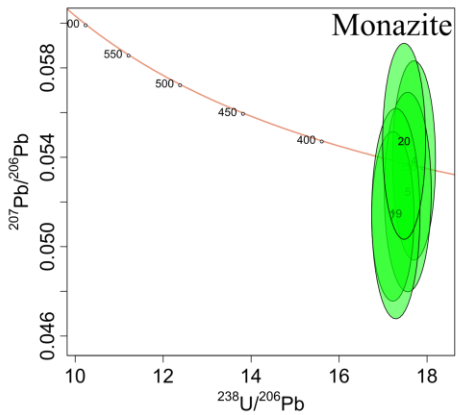

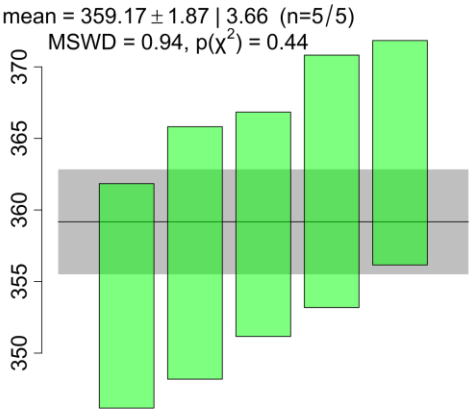

14 e) Petalinka Waterfall: A150503A

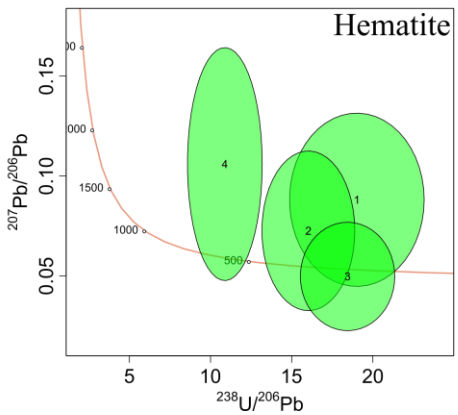

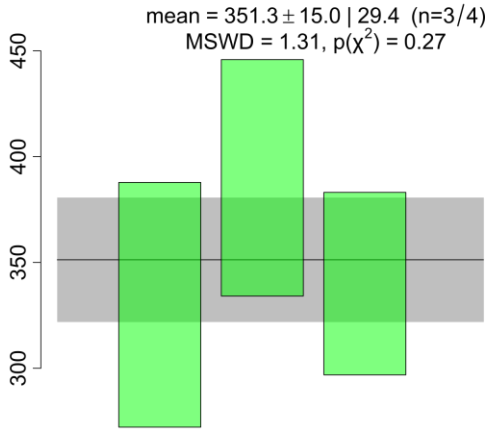

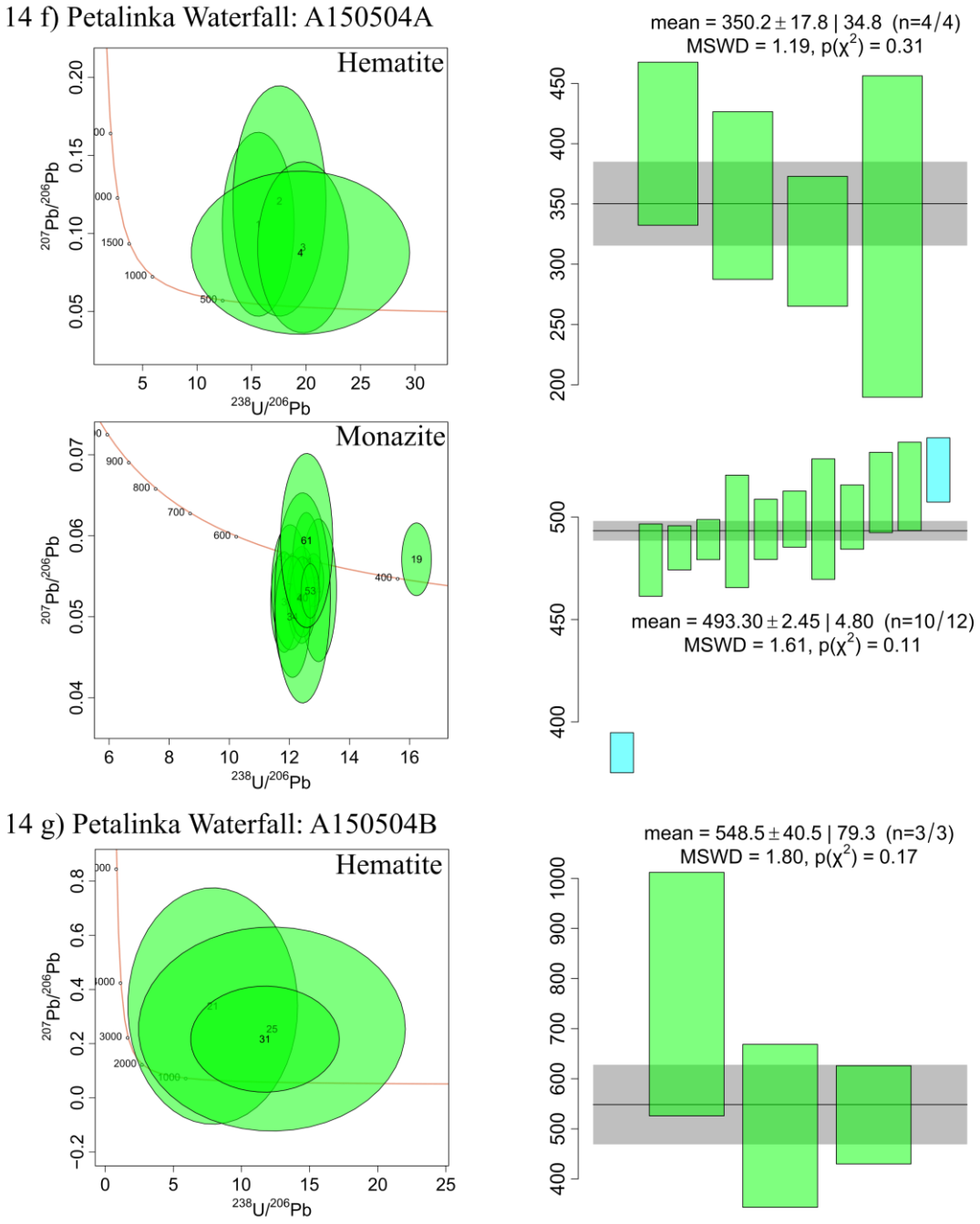

Figure 14. Concordia plots with calculated age histograms. Blue data points signify outlier data points and were filtered from age calculation.

Table 3. Table of geochronology data from hematite and monazite dating. *No datable monazite found in sample. **Hematite dating values unreliable due to inclusions or low uranium content.

Sample	Location	Hematite Date	+/-	Monazite Date	+/-
A160501A	Radium Ridge	305	5	363.9	0.94
A160501B	Radium Ridge	295	4	363.12	0.85
A160506	Mt Gee	313	5	368.02	1.72
Mt Gee A	Mt Gee	**		359.17	1.87
Mt Gee B	Mt Gee	**		*	
A150501A	Petalinka Waterfall	**		*	
A150503A	Petalinka Waterfall	351	15	*	
A150504A	Petalinka Waterfall	350	18	493.3	2.45
A150504B	Petalinka Waterfall	549	41	*	
MasHem	Mt Oliphant	**		*	
QHV	Mt Oliphant	**		*	
A150507E	Mt Oliphant	**		*	

Hematite dates from Radium Ridge and Mt Gee are all ca 300 Ma, with monazite dates at ca 360 Ma. This suggests a potential resetting of hematite ages or, different timing of formation of these mineral phases. Monazite dates from Radium Ridge and Mt Gee are within error of the monazite dates reported by Hore, (2020). The monazite populations from Radium Ridge had large variability within the samples (Figure 14a-b), which suggests the resetting of monazite crystals. In this case, outlier monazite populations were filtered out prior to age calculations. Petalinka Waterfall hematite samples return two dates of ca 350 Ma and one date of ca 550 Ma. A monazite date from 150504A is close to within error of the outlier hematite date at ca 490 Ma suggesting a hematite resetting events in the region. The similar ages from the hematite and monazite are from samples located within 1 metre of each other and are assumed to be of the same system. Unfortunately, hematite samples from Mt Oliphant did not have sufficient uranium

content to return concordant data and these samples did not contain monazite. Therefore, these samples remain undated.

DISCUSSION

Mt Gee and Radium Ridge Relationship

The Mt Gee sinter and Radium Ridge breccia are genetically related, according to Stillwell and Edwards (1945). Geochronological evidence from hematite and monazite dating (Table 3) suggests a potential resetting of hematite or asynchronicity between hematite and monazite formation within the Mt Gee sinter and Radium Ridge breccia. The repeated pulses from the British Empire granite at ca 400 and 330 Ma (McLaren, et al. 2002) and multiple generations of hydrothermal activity at Mt Gee is an explanation for this difference. The first generation, euhedral hematite likely predates the monazite in these samples as all monazite from Mt Gee presides within the second generation of hematite and quartz. Therefore, hematite mobilisation likely predates the ca 360 Ma date of monazite further expanding the range of hydrothermal activity within the Mt Gee Sinter. This is also potentially evident from the large spread of concordant monazite population from the Mt Gee and Radium Ridge samples (Figures 13a-d). However, this could also be an artefact of continued hydrothermal activity or Pb exchange and leaching, resetting or altering the monazite grains as well. The coexistence of hematite and monazite within the same generation suggests a resetting of hematite must take place. The failed $\delta^{18}O$ results, returning impossible fluid temperatures from Mt Gee and Radium Ridge samples imply a disequilibrium between hematite and quartz. This further supports the hypothesis of potential resetting of already crystalline minerals in the region. The congruency between the hematite and

monazite dates between the Mt Gee and Radium Ridge samples suggests that the conditions between the two locations were coupled. The REE pattern of the Radium Ridge monazite samples display two distinct monazite populations with differing HREE content, most notably in Figure 13a, backing up the claim of local monazite resetting and alteration. The genetic relationship of the Mt Gee sinter and the Radium Ridge Breccia suggested by Stillwell and Edwards (1945) is also supported by the hematite trace element content with the general trace element pattern matching across all samples from Mt Gee and Radium Ridge (Figure 12). The evolving hydrothermal conditions in the region started before ca. 360 Ma with the monazite poor generation of hematite from Mt Gee and continued to form and alter the breccia and sinter at Radium Ridge and Mt Gee until at least ca. 300 Ma. Hydrothermal activity evolved and continued in the region with the hematite poor generation of quartz, known as the Nail-hole quartz with evidence of cross-cutting of Cretaceous Diamictite, suggesting a maximum age of hydrothermal activity of ca. 220 Ma. (Hore, 2020).

Petalinka Waterfall and Mt Oliphant Relationship

Petalinka Waterfall and Mt Oliphant lie within the Neoproterozoic metasediments and therefore, the localities have similar metamorphic histories. The trace element content of hematite grains (Figure12) from Petalinka Waterfall and Mt Oliphant are relatively congruent, suggesting a common source of hydrothermal fluid transporting these elements. This is typified by high Mg, Ti, V, and Cr concentrations and low REE concentrations, when compared to the Mt Gee and Radium Ridge samples. This suggestion of a genetic relationship is also supported by petrogenic and physical characteristics and relationships of the hydrothermal veins themselves. The monazite REE plot (Figure 13e) from Petalinka Waterfall is similar to the monazite REE plots

from Mt Gee and Radium Ridge, suggesting a consistent abundance of REE in the region. Although geochronology results were unsuccessful in correlating vein formation across the two regions, a distinct presence of multiple generations of veining links the two regions. The metasedimentary rocks hosting these hydrothermal veins have been deformed throughout the late Neoproterozoic, culminating with the Delamarian Orogeny (Morphett, 2013). The first generation of hematite and quartz veins at Mt Oliphant is foliated heavily with the Woodnamocka Phyllite host rock. The Woodnamocka Phyllite has multiple generations of foliation and deformation fabric. The first fabric is interpreted to predate monazite and cordierite growth at ca 705 Ma (Morphett, 2013). The second deformation event overprints the previous fabric and postdates the deposition of the Pound Quartzite, from the youngest stratigraphic layer of the Wilpena Group from the Adelaidean (Morphett, 2013). This suggests the foliation is at most ca 550 Ma and likely part of the Delamarian Orogeny deformation, closer to ca 500 Ma (Foden, et al. 2006). This first generation of veining was unsuccessfully U-Pb dated, but with the consideration of the age of the foliation within the host rock, these veins must be older than approximately ca 500-550 Ma. At Petalinka Waterfall, a hematized section of veining, rich in biotite (sample A150504A) returned monazite dates of 493 +/-3 Ma. This suggests a potential correlation between the first-generation veins at Mt Oliphant and this set of veins at Petalinka Waterfall. Hematite dates from a sample of the same outcrop (sample A150504B) returned a date of ca 549, within the range of the deformation within the region. Therefore, this set of hematite and quartz veins from Petalinka Waterfall, as well as the first-generation of veins at Mt Oliphant, are likely associated with the Delamarian Orogeny. Sample A150504A was heavily hematized, and the hematite within this sample was dated at ca 350 Ma. Separate veins

from Petalinka Waterfall also return a date of ca 351 Ma suggesting further hydrothermal fluid activity contributed to hematization of the area as well as deposition of more hematite and quartz veins. The second generation of hematite and quartz at Mt Oliphant was unsuccessfully dated as well, however, this set of veins overprint existing foliation as well as the first generation of veining. Due to the relationship of the veins at Petalinka Waterfall and Mt Oliphant, this second generation of veins at Mt Oliphant are suggested to be related to the younger set of veining and hematization at Petalinka Waterfall, however, further work is needed to accurately confine this observation. Monazite and hematite date congruency between samples at Petalinka Waterfall, Mt Gee and Radium Ridge suggest the same system causes hydrothermal fluid transport across the region. This system is likely from the pulses from the ca 400 - 330 Ma British Empire Granite (McLaren, et al. 2006).

Regional Hydrothermal Chronology

Events discussed above suggest approximate 150 Ma and 240 Ma phases of periodic hydrothermal activity within the Adelaidean metasediments and the Mt Painter Inlier respectively. The veins presiding within the Adelaidean metasediments at Petalinka Waterfall and Mt Oliphant initiated prior or during the orogenic conditions from the Delamarian Orogeny at ca 515-490 Ma. The Mt Painter Inlier's hydrothermal history initiated with the magmatic to hydrothermal transition at ca. 440 Ma studied by Bakker and Elburg (2006), with the Alice Springs Orogeny and associated British Empire granite intrusion. These highly saline diopside-titanite forming intrusions evolved to less saline hematite and quartz forming hydrothermal veins (Bakker and Elburg, 2006). Uranium baring ore from the Radium Ridge Breccia is also dated at ca 440 (Elburg, 2012), followed by major hydrothermal activity at approximately ca 360 Ma with the

further development of the Radium Ridge Breccia and the Mt Gee sinter (Hore, 2020). Monazite dates from Radium Ridge ore samples and Mt Gee from this study correlate with this ca 360 Ma date, however, associated hematite dates suggest a resetting event locally at Mt Gee closer to 300 Ma. Hematite dates from Petalinka Waterfall suggest this ca 360 Ma hydrothermal event was much more regional with both Mt Painter inlier and Adelaidean Sediment veins forming concurrently. Local hydrothermal events at the Mt Gee Sinter, within the Mt Painter Inlier continued until at least ca 220 Ma following deposition of the Sprigg Tillite (Hore, 2020). Figure 15 represents the major hydrothermal timeline for the Mt Painter Inlier and Adelaidean Sediments at Arkaroola with hematite and monazite dates from this study.

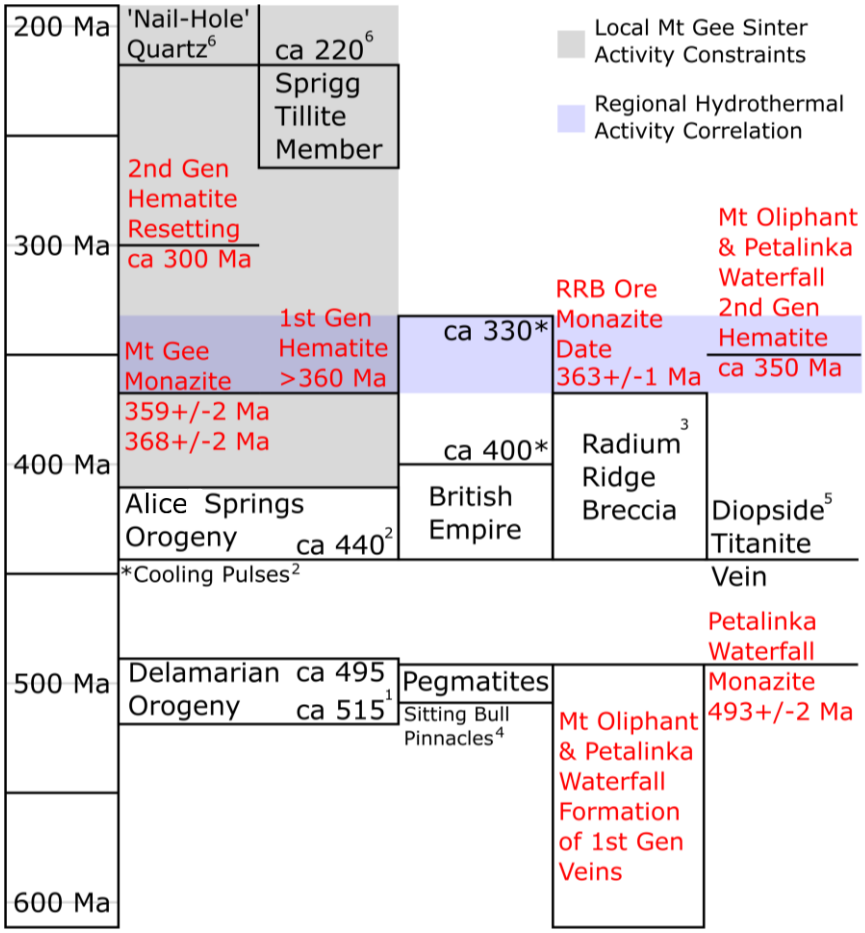

Figure 15. Stratigraphic column of known relevant ages of magmatic and hydrothermal events with dates from this paper highlighted in red. 1. Delamarian Constraints by Foden (2006). 2. Alice Springs Orogeny timing by McLaren (2002). 3. Timing of RRB by McLaren (2006). 4. Pegmatites in Region by Elburg (2013). 5. Diopside and titanite veins from Bakker & Elburg (2006). 6. Cretaceous Tillite by Hore (2020).

Vein Transect and Mt Oliphant

A geochemical transect from chloritic altered rock associated with veining to unaltered host rock close and distal to the veins were used to establish the alteration effect of these hydrothermal veins on the host rock. This chloritic alteration was only present at the veins within the Woodnamocka Phyllite at Mt Oliphant. Other vein outcrops saw hematite alteration instead. This is likely due to the phyllite host rock being rich in Al and Mg. Immediate observations from in the field show that the veins heavily altered the host rock within an approximate 2 metre area surrounding the veins. The hematite alteration was more varied depending on the host rock. Formations such as the Shanahan Conglomerate were significantly more altered with areas of the conglomerate being completely hematized within a 10 square metre area. Whereas the Paralana Quartzite was much more locally altered around the hydrothermal veins. Bulk geochemical analysis of a transect from the Mt Oliphant series of veins shows an immediate enrichment of Fe_2O_3 and depletion in most other major oxides in the host rock. This is not surprising, due to the hydrothermal fluid carrying large concentrations of iron that leech into the host rock. The enrichment of only iron in the host rock suggests the fluid was enriched in only iron, which also explains why only hematite forms from these veins.

Fluid Conditions

As suggested by Bakker and Elburg (2006) and Cabral (2013), Fe^{3+} can be mobilised in hydrothermal systems that are highly saline. Bakker and Elburg (2006) discuss a highly saline, magmatic-related fluid phase responsible for titanite and diopside vein growth followed by a reduction in salinity and a transition into a purely hydrothermal system. This process is dated at ca 440 Ma with the hydrothermal system following directly

after the magmatic phase. Due to the proximity of approximately 1-2 km of this set of veins from Mt Gee and Radium Ridge, the later hydrothermal phase may be remobilised with the continued pulses from the British Empire Granite, suggesting these veins are genetically related. Formation conditions of the magmatic phase from the Bakker and Elburg (2006) study are at 510 +/- 20^{o}C and 130 +/- 10 MPa and cooling to 350 +/- 20^{o}C and 80 +/- 10 MPa at the hydrothermal phase. δ^{18}O isotope value calculations (Table 2) show the Radium Ridge set of hematite breccia reached temperatures of 400 to 500 ºC, which is similar to than suggested by Bakker and Elburg (2006). The range of δ^{18}O values from the samples at Mt Gee and Radium Ridge may be a result of meteoric fluid contamination circulating through fault lines or porous rock lowering δ^{18}O values. This δ^{18}O contamination could also be achieved from host rock oxygen isotope leaching/exchange from high temperature fluids altering host rock, increasing δ^{18}O values. Metamorphic fluid from the heating of evaporite sediments such as the Woodnamocka Phyllite is a potential source of this fluid within the Neoproterozoic sediment veins. Further study focussing on fluid inclusion salinity, similar to Bakker and Elburg (2006) could further develop this theory and confine salinity values for these veins. The hydrothermal systems at Mt Gee and Radium Ridge are likely not genetically related to those at Petalinka Waterfall and Mt Oliphant due to the difference in trace element abundances. However, this could be due to contamination of host rock as the veins are found within separate lithology groups. The hydrothermal activity at ca 360 Ma is likely temporally related due to the temperature pulses of the British Empire Granite (McLaren, 2006). Table 2 shows temperatures of hydrothermal fluid through oxygen isotope data. This shows that samples from Petalinka Waterfall are approximately 450-500^{o}C while samples at Mt Oliphant are approximately around

600ºC. This could be due to the local geothermal gradient that led to formations of cordierite within the Woodnamocka Phyllite at peak metamorphism, due to the local Wooltana Volcanics. This could also be an artafact of the large variability of $\delta^{18}O$ values from Mt Oliphant and Petalinka waterfall, again, potentially due to contamination of $\delta^{18}O$ values from host rock leaching or alteration. The hydrothermal fluid likely cooled slowly, due to the large usually decimetre to centimetre scale, euhedral nature of the veins. These low temperature conditions lead to very acicular laumontite crystal formation at Mt Gee. This low temperature mineral at the youngest stage of hydrothermal activity requires a very gentle, low temperature flowing slurry of quartz to allow for the laumontite crystal growth and rapid exhumation of low temperature fluid to preserve this mineral texture.

CONCLUSIONS

Hematite and quartz veins from Mt Gee and Radium Ridge are likely genetically related and experience the same hydrothermal activity. This is evident through geochronology dates of monazite formation at ca 360 Ma, and potential hematite resetting at ca 300 Ma. This was evident across both sample locations as well as trace element concentrations linking the two locations. Hematite and quartz veins at Petalinka Waterfall and Mt Oliphant are also likely genetically related to one another, due to correlations between host rock and vein interactions and trace element abundances. Uranium – Lead dating was unsuccessful in correlating the two locations temporally, but petrological and structural evidence helps relate two generations of veins across the two regions. The first generation of veining is suggested to be congruent with the Delamarian Orogeny at ca 515-495 Ma due to structural evidence of vein foliation

within the Woodnamocka Phyllite at Mt Oliphant, as well as monazite dating from a sample at Petalinka Waterfall. The second generation of hematite and quartz veins at Petalinka Waterfall and Mt Oliphant are also likely from the same system at ca 350 Ma. Veins formation at Mt Gee, Radium Ridge, Petalinka Waterfall and Mt Oliphant likely activated from the same system as geochronology has linked the two areas. Further geochronological research should be undertaken to confirm these observations. Overall hydrothermal conditions across both systems are likely similar to the pure hydrothermal phase from Bakker and Elburg (2006). This was a highly saline fluid at around 350^{o}C +/- 20. Temperatures could be higher across the study sites with δ^{18}O sample analysis returning temperatures of approximately 450^{o}C and 600^{o}C, however, these results could be artafacts of δ^{18}O contamination. Further exploration of δ^{18}O of other minerals and with more samples could help further constrain fluid temperature conditions of the region.

ACKNOWLEDGMENTS

I would firstly like to thank my supervisor, Carl Spandler for guiding me through this year as well as providing valuable feedback throughout the thesis writing process. I would also like to thank Stephen Hore for this valuable and extensive knowledge of the Arkaroola area and for guiding us with our fieldwork and thanks to Mistrel Fetzer Boegheim for her help in the field. I also thank the Sprigg Family and the staff at the Arkaroola Village for their fantastic hospitality. A big thanks to Katie Howard for assisting the honours group with all sorts of requests and finding lab gear in the dark corners of the Mawson Building. A big thank you to the Adelaide Microscopy staff, namely, Ken Neubauer for training and assistance with the SEM and Sarah Gilbert for training and assistance with the LA-ICP MS. Lasty, a massive thank you to all of the honours students for making this year one to remember.

REFERENCES

Armit R. J., Betts, P. G., Schaefer, B. F., Pankhurst, M. J., Giles, D. 2014 Provenance of the Early Mesoproterozoic Radium Creek Group in the northern Mount Painter Inlier: Correlating isotopic signatures to inform tectonic reconstructions, *Precambrian Research,* vol. 243, pp. 63-87.

Bakker R. & Elburg M. A. 2006 A magmatic-hydrothermal transition in Arkaroola (northern Flinders Ranges, South Australia): From diopside-titanite pegmatites to hematite-quartz growth, *Mineral Pertrology,* vol. 152, no. 5, pp. 541-569.

Ballèvre M., Möller A. & Hensen B. J. 2000 Exhumation of the lower crust during crustal shortening: an Alice Springs (380 Ma) age for a prograde amphibolite facies shear zone in the Strangways Metamorphic Complex (central Australia), *Journal of Metamorphic Geology,* vol. 18, no. 6, pp. 737-747.

Brugger J., Krivovichev, S. V., Berlepsch, P., Meisser, N., Ansermet, S., Armbruster, T. 2004 Spriggite, Pb3 [(UO2)6O8(OH)2] (H2O)3, a new mineral with β-U3O8 –type sheets: Description and crystal structure, *American Mineralogist,* vol. 89, no. 2-3, pp. 339-347.

Cabral A. & Rosière C. 2013 The chemical composition of specular hematite from Tilkerode, Harz, Germany: Implications for the genesis of hydrothermal hematite and comparison with the Quadrilátero Ferrífero of Minas Gerais, Brazil, *Mineralium Deposita,* vol. 48.

Drexel J. F., Priess W. V. & Parker A. 1993 The Geology of South Australia. Mines and Energy, South Australia, Geological Survey of South Australia.

Elburg M. A., Bons, P. D., Foden, J., Brugger, J. 2003 A newly defined Late Ordovician magmatic–thermal event in the Mt Painter Province, northern Flinders Ranges, South Australia, *Australian Journal of Earth Sciences* vol. 50, pp. 611-631.

Elburg M. A., Andersen, T., Bons, P. D., Weisheit, A., Simonsen, S. L., Smet, I. 2012 Metasomatism and metallogeny of A-type granites of the Mt Painter–Mt Babbage Inliers, South Australia, Lithos, vol. 151, pp. 83-104.

Elburg M. A., Andersen, T., Bons, P. D., Simonsen, S. L., Weisheit, A. 2013 New constraints on Phanerozoic magmatic and hydrothermal events in the Mt Painter Province, South Australia, *Gondwana Research,* vol. 24.

Foden J., *Elburg, M. A., Dougherty-Page, J., Burtt, A.* 2006 The Timing and Duration of the Delamerian Orogeny: Correlation with the Ross Orogen and Implications for Gondwana Assembly, *The Journal of Geology,* vol. 114, pp. 189-210.

Harris C. & Vogeli J. 2010 Oxygen isotope composition of garnet in the Peninsula Granite, Cape Granite Suite, South Africa: Constraints on melting and emplacement mechanisms, *South African Journal of Geology,* vol. 113.

Hore S., Reid A. & Hill S. M. 2015 Definition and age of the enigmatic Sprigg Diamictite Member, northern Flinders Ranges, South Australia, *MESA Journal,* vol. 77, pp. 42-54.

Hore S. B., Hill, S. M., Reid, A., Wade, B., Alley, N. F., Mason, D. R. 2020 U–Pb geochronology reveals evidence of a Late Devonian hydrothermal event, and protracted hydrothermal–epithermal system, within the Mount Painter Inlier, northern Flinders Ranges, South Australia, *Australian Journal of Earth Sciences,* vol. 67, no. 7, pp. 1009-1044.

Job A. 2011 Evolution of the basal Adelaidean in the northern Flinders Ranges: deposition, provenance and deformation of the Callanna and lower Burra Groups. School of Earth and Environmental Sciences University of Adelaide.

Lloyd J. C., Blades, M. L., Counts, J. W., Collins, A. S., Amos, K. J., Wade, B. P., Hall, J. W., Hore, S., Ball, A. L., Shahin, S., Drabsch, M. 2020 Neoproterozoic geochronology and provenance of the Adelaide Superbasin, *Precambrian Research,* vol. 350, p. 105849.

M. A. Elburg P. D. B., J. Foden, J. Brugger 2003 A newly defined Late Ordovician magmatic–thermal event in the Mt Painter Province, northern Flinders Ranges, South Australia, *Australian Journal of Earth Sciences,* vol. 50, pp. 611-631.

McDonough W. & Sun S. 1995 The composition of the Earth, *Chemical Geology,* vol. 120, pp. 223-253.

McLaren S., Dunlap, W. J., Sandiford, M., McDougall, I. 2002 Thermochronology of high heat-producing crust at Mount Painter, South Australia: Implications for tectonic reactivation of continental interiors, *Tectonics,* vol. 21, no. 4, pp. 2-1-2-18.

McLaren S., Sandiford, M., Powell, R., Neumann, N., Woodhead, J. O. N. 2006 Palaeozoic Intraplate Crustal Anatexis in the Mount Painter Province, South Australia: Timing, Thermal Budgets and the Role of Crustal Heat Production, *Journal of Petrology,* vol. 47, no. 12, pp. 2281-2302.

Morphett W. J. 2013 Geochronological and Structural insights into the evolution of the Lower Burra and Callana Groups near Arkaroola: Structural mapping and U-Pb metamorphic monazite dating. School of Earth and Environmental Sciences. University of Adelaide.

Paul E., Flöttmann T. & Sandiford M. 1999 Structural geometry and controls on basement-involved deformation in the northern Flinders Ranges, Adelaide Fold Belt, South Australia, *Australian Journal of Earth Sciences,* vol. 46, no. 3, pp. 343-354.

Robinson M. L. 1998 Characterization of different vein types and their local settings near the basement - Cover contact of the mount painter inlier, South Australia.

Sandiford M., Paul E. & Flottmann T. 1998 Sedimentary thickness variations and deformation intensity during basin inversion in the Flinders Ranges, South Australia, *Journal of Structural Geology,* vol. 20, no. 12, pp. 1721-1731.

Slezak P. & Spandler C. 2020 Petrogenesis of the Gifford Creek Carbonatite Complex, Western Australia, *Contributions to Mineralogy and Petrology,* vol. 175.

Stillwell F. L. & Edwards A. B. 1951 Mineralogical Society (London), *American Mineralogist,* vol. 36, no. 3-4, pp. 357-357.

Vho A., Lanari P. & Rubatto D. 2019 An Internally-Consistent Database for Oxygen Isotope Fractionation Between Minerals, *Journal of Petrology,* vol. 60, no. 11, pp. 2101-2129.

Warren J. K. 2015 Evaporites: A Geological Compendium. (Second edition). Springer

Weisheit A., Bons P. D. & Elburg M. A. 2013 Long-lived crustal-scale fluid flow: the hydrothermal mega-breccia of Hidden Valley, Mt. Painter Inlier, South Australia, *International Journal of Earth Sciences,* vol. 102, no. 5, pp. 1219-1236.

ZHENG F. & SIMON K. 1991 Oxygen isotope fractionation in hematite and magnetite: A theoretical calculation and application to geothermometry of metamorphic iron-formations *European Journal of Mineralogy,* vol. Volume 3, no. 5, pp. 877-88